Maturation and detoxification of synphilin-1 inclusion bodies regulated by sphingolipids

Xiuling Cao[1,2]†, Xiang Wu[1]†, Lei Zhao[2]†, Ju Zheng[2,3], Xuejiao Jin[1], Xinxin Hao[2], Joris Winderickx[3], Shenkui Liu[1], Lihua Chen[2,4]*, Beidong Liu[1,2]*

[1] State Key Laboratory of Subtropical Silviculture, Zhejiang A&F University, Hangzhou, China. [2] Department of Chemistry and Molecular Biology, University of Gothenburg, Gothenburg, Sweden. [3] Functional Biology, KU Leuven, Leuven, Belgium. [4] Guangzhou Laboratory, Guangzhou, Guangdong, China.

† These authors contributed equally to this work.

* Corresponding author. Email: beidong.liu@cmb.gu.se (B.L.); chen_lihua@gzlab.ac.cn (L.C.)

Abstract

Due to proteostasis stress induced by aging or disease, misfolded proteins can form toxic intermediate species of aggregates and eventually mature into less toxic inclusion bodies (IBs). Here, using a yeast imaging-based screen, we identified 84 potential synphilin-1 (SY1) IB regulators and isolated the conserved sphingolipid metabolic components in the most enriched groups. Furthermore, we show that, in both yeast cells and mammalian cells, SY1 IBs are associated with mitochondria. Pharmacological inhibition of the sphingolipid metabolism pathway or knockout of its key genes results in a delayed IB maturation and increased SY1 cytotoxicity. We postulate that SY1 IB matures by association with the mitochondrion membrane, and that sphingolipids stimulate the maturation via their membrane-modulating function and thereby protecting cells from SY1 cytotoxicity. Our findings identify a conserved cellular component essential for IB maturation and suggest a mechanism by which cells may detoxify the pathogenic protein aggregates through forming mitochondrion-associated IBs.

Introduction

Proteins are vulnerable macromolecules and are often endangered by misfolding and aggregation during the life of the cell due to destabilizing mutations, stress conditions or unique metabolic challenges that occur during aging or disease (Buchberger et al., 2010; Hartl and Hayer-Hartl, 2009). To cope with protein damage and in order to survive, the eukaryotic cell has evolved complex protein quality control systems that monitor and maintain the integrity of its proteome, including refolding, degradation and sequestration (Buchberger *et al.*, 2010; Frydman, 2001; Hartl and Hayer-Hartl, 2009; Lim and Yue, 2015). The refolding of stress-denatured proteins and the degradation of misfolded proteins are assisted by molecular chaperones (Chen et al., 2011; Hartl and Hayer-Hartl, 2009). In addition to refolding and degradation, cells have another cellular strategy to cope with an overload of aberrant proteins or toxic intermediate species of aggregates, namely sequestration into specialized quality control IBs (Bagola and Sommer, 2008; Kaganovich et al., 2008; Kopito, 2000).

It has become increasingly clear that the formation of IBs is like a "triage" center, thus being protective machinery against proteostasis stress during aging or disease. Therefore, the inability to form IBs would poison the intracellular environment and cause cell dysfunction or even death (Lim and Yue, 2015). The toxicity of protein aggregates is more pronounced in neurons partly due to their unique cellular architecture. Indeed, mounting evidence has linked a number of neurodegenerative diseases including Alzheimer's disease (AD), Parkinson's disease (PD), Huntington's disease (HD) and amyotrophic lateral sclerosis (ALS), to the formation of misfolded proteins aggregates containing IBs (Ross and Poirier, 2004). Although IBs have been extensively studied, including their unique characteristics (Kaganovich *et al.*, 2008; Ogrodnik et al., 2014; Weisberg et al., 2012) and the IB clearance machinery (Moldavski et al., 2015), the genes and cellular components that regulate the IB maturation remain poorly understood. In addition, we have little insight into the effects of IBs on cellular membrane-bound structures as IBs have been found to interact with membrane domains (Büttner et al., 2010).

SY1 contributes to inclusion formation and has been implicated in the pathogenesis of PD, an incurable, progressive neurodegenerative disorder. The biological functions of SY1 are not fully understood, and whether SY1 is cytotoxic or protective remains controversial. In aged yeast cells, SY1 expression reduced survival and triggered apoptosis and necrotic cell death in a Sir2 dependent manner (Büttner *et al.*, 2010). However, SY1 exerted neuroprotective effects by inhibiting reactive oxygen species (ROS) production and apoptosis in an *in vitro* PD model (Shishido et al., 2019), and SY1 attenuated mutant LRRK2-induced PD-

like phenotypes and played a neuronal protective role in cultured cells and *Drosophila* (Liu et al., 2016). Transgenic mice expressing SY1 caused pathological inclusions and degeneration of dopaminergic neurons in the substantia nigra (Krenz et al., 2009), and reduced motor skill learning and motor performance (Jin et al., 2008; Nuber et al., 2010). In contrast, SY1 overexpression in A53T human α-synuclein (α-Syn) transgenic mice reduced astrogliosis and neuronal degeneration, resulting in increased lifespan(Smith et al., 2010). In an aged A30P α-Syn transgenic mouse model, Casadei *et al* observed that overexpression of SY1 promoted clearance of soluble and misfolded α-Syn, but did not rescue the motor deficit phenotype (Casadei et al., 2014).

Given that a high-content imaging approach has been successfully conducted for SY1 (Zhao et al., 2016), it was possible to study on a genome-wide scale the cellular components that are involved in IB formation by using yeast as a model. Moreover, since SY1 binds phospholipids, membranes, lipid droplets and synaptic vesicles (Ribeiro et al., 2002; Takahashi et al., 2006) and given that the membrane-binding properties of α-Syn are thought to be relevant for its pathological activity, we speculated that also for SY1 the binding to different types of lipid structures might be related to its cytotoxicity. Here we combined the SGA approach with a high-content imaging-based screen to survey the genetic mutants with altered SY1 aggregation types using a yeast genome-wide mutant library. We identified the conserved sphingolipid metabolic pathway as an essential component for the maturation of SY1 IBs and for the detoxification of SY1 aggregates. In the sphingolipid-rich endomembrane system, SY1 aggregates tightly interact with mitochondria. Disruption of sphingolipid synthesis prevented this association, resulting in small, dispersed aggregates and enhanced SY1-induced cytotoxicity, notably mitochondrial toxicity. Furthermore, pharmacological inhibition of the sphingolipid pathway or knockdown of SPTLC2 altered the morphology of SY1 IBs and increased their cytotoxicity in mammalian cells, and this could be reversed by increasing the level of dihydrosphingosine (DHS), a sphingolipid synthesis intermediate.

Results

SY1 IB management in yeast cells

The formation of SY1 IBs in the yeast (*Saccharomyces cerevisiae*) has been studied by expressing the protein (DsRed-SY1) with a plasmid pYX212 under the control of a constitutive *TPI1* promoter(Zhao *et al.*, 2016).

83 Using a similar approach, we observed different phenotypes of SY1 aggregates in yeast cells. During the lag
84 phase (4 h), multiple small IBs presented in the cytoplasm but in the exponential growth phase (16 h), these
85 small aggregates merged into larger IBs, resulting in a decreased number of smaller aggregates. Subsequently,
86 when the cells entered the stationary phase (48 h), most of the SY1-expressing cells retained only one to a
87 few large IBs (Figure 1A). Thus, consistent with previously reported data (Büttner *et al.*, 2010), this time-
88 course study demonstrated a maturation process of SY1 IBs in yeast cells. To study the details of this process,
89 we defined the IB phenotypes as Class 1 (one aggregate in a cell), Class 2 (two aggregates in a cell), and
90 Class 3 (three or more aggregates in a cell), respectively (Figure 1B), as previously reported for mutant
91 huntingtin inclusions (Yang et al., 2016). We then monitored the SY1 IBs every 4 hours from 4 to 48 hours.
92 Most of the SY1 IB-forming cells exhibited a Class 3 phenotype (96%) at the 4-hour time-point. During
93 growth, the proportion of Class 3 ratio dropped over time, while the proportion of Class 1 and Class 2 ratios
94 increased inversely. After 24 hours, the proportions became stable and Class 1 IBs accounted for
95 approximately 50% when cells reached stationary phase (Figure 1C). All these observations supported the
96 notion that there is a compartmentalization process of SY1 IBs in the yeast cell. We therefore hypothesized
97 that the formation and maturation of IBs is a cytoprotective process that helps sequester more toxic
98 aggregates/oligomers into larger inert deposits (Kitamura et al., 2006).

99 Dysregulation of the formation of pathogenic protein inclusions is the major hallmark of age-related
100 neurodegenerative diseases. To investigate whether IBs formed by SY1 expression in old cells have the same
101 maturation process as that in young cells. We isolated old cells and examined the SY1 aggregates in old cells
102 (≥5 generations) and young cells (≤1 generation) (Figure 1D). In young cells, about 27% cells had SY1
103 inclusions while in the old cells the ratio increased to 61% (Figure 1E). Furthermore, when counted the
104 number of aggregates in individual cells, we found that there were much more aggregates per cell in the old
105 cell population (Figure 1F, 4.91±3.32 of old cells vs 2.64±1.29 of young cells). These findings suggested
106 that there was a dysregulation of SY1 IB maturation in old cells. However, the underlying mechanism
107 remains unclear. This motivated us to further investigate the genes and cellular components that regulate
108 SY1 IB maturation.

109 **Genome-wide screening for cellular components regulating the maturation of SY1 inclusions**

110 To dissect the genes and cellular components that mediate the maturation of IBs, a genome-wide, high-
111 content imaging-based screening approach was performed (Zhao *et al.*, 2016) (Figure 2A). Prior to

112 performing the screen, we determined the appropriate time-point to assess the phenotypes of SY1 IBs. As
113 shown in Figure 1A-C, at 16-20 hours of growth (OD_{600} is 3.0 ~ 4.0), approximately 50% SY1-expressing
114 cells had Class 3 aggregates, and the ratios were stable thereafter. Therefore, we chose the time point 20-
115 hours for the following screening and other studies. We set the same criteria as in the previous study (Zhao
116 *et al.*, 2016) to include a particular mutant strain as a potential hit if: 1) the difference in the number of cells
117 with Class 3 SY1 IBs between wild-type and mutant cells is statistically significant ($P \leq 0.05$, *t*-test) and 2)
118 the absolute difference of the percentage of wild-type and mutant cells carrying SY1 inclusions is at least
119 20%. Potential hits acquired from the screening were then confirmed by manual examination of the Class 3
120 inclusion phenotype using a microscopic approach.

121 The screen was performed three times independently. Based on the above criteria and subsequent manual
122 confirmation, a list of 84 mutants that showed an increase in cells carrying Class 3 SY1 IBs was obtained
123 (Supplementary file 1). GO enrichment analysis indicated that these mutants were enriched in the following
124 modules: serine C-palmitoyltransferase (SPT) complex, SPOTS complex, protein urmylation, TORC2
125 complex, palmitoyltransferase complex, and others (Figure 2B and 2C). The complete list of GO terms can
126 be found in Supplementary file 2. Among them, SPT complex and SPOTS complex, containing LCB1, LCB2
127 and TSC3 had the highest enrichment (Table S2, Figure 2B and 2C), corresponding to the mutants including
128 *lcb1-4*, *lcb2-1*, *lcb2-2* and *tsc3-2* in our screen. We performed gene complementation experiments on three
129 mutants *lcb1-4*, *lcb2-1* and *tsc3-2*. Restoring the corresponding gene almost completely rescued the SY1 IB
130 phenotype with significantly reduced Class 3 IBs (Figure 2D and 2E). Thus, our above screen suggested a
131 link between the highly conserved sphingolipid metabolic pathway and the maturation of SY1 IBs. A
132 substantial body of evidence has highlighted an important role of sphingolipid metabolism in several
133 neurodegenerative diseases, including Alzheimer's disease (Mielke and Lyketsos, 2010), amyotrophic lateral
134 sclerosis(Cutler et al., 2002), and Parkinson's disease (France-Lanord et al., 1997). Therefore, we aimed to
135 elucidate the functional role of sphingolipid metabolism in the regulation of SY1 IB maturation and
136 cytotoxicity.

137 **Sphingolipids regulate SY1 IB maturation and cytotoxicity in yeast cells**

138 The first step of intracellular sphingolipid de novo synthesis is identical in both yeast and humans, with
139 palmitoyl-CoA and serine catalyzed by the SPT complex to form 3-Ketosphinganine, which could be
140 blocked by myriocin (Figure 3A). 3-ketosphinganine is subsequently catalyzed to dihydrosphingosine

141 (DHS), and dihydroceramide, and further converted into complex sphingolipids. We first confirmed that
142 exogenous addition of DHS in SPT mutants (*lcb1-4*, *lcb2-1* and *tsc3-2*) could rescue the phenotype of
143 increased Class 3 SY1 IBs (Figure 3B and 3C). In addition, blockade of intracellular sphingolipid
144 metabolism pathways by myriocin strongly perturbed SY1 IB maturation process, resulting in elevated Class
145 3 IBs (Figure 3D and 3E). Again, addition of exogenous DHS could suppress the myriocin-induced Class 3
146 aggregates (Figure 3D and 3E). Next, we tested whether the SPT genes could regulate SY1 cytotoxicity in
147 yeast cells. Expressing SY1 did not cause dramatic growth defect in wild-type cells, but led to severe growth
148 defects in the SPT mutants (Figure 3F, left). Furthermore, this defect could also be rescued by the addition
149 of DHS (Figure 3F, right). Taken together, these data suggest that sphingolipids may help cells reduce the
150 cytotoxicity of protein aggregates by regulating the IB maturation process. These findings motivated us to
151 further unravel the underlying mechanism by which sphingolipids regulate the maturation process and
152 cytotoxicity of SY1 IBs.

153 **SY1 IBs associate with mitochondria in yeast cells**

154 Sphingolipids are structural molecules of cell membranes that play an important role in maintaining barrier
155 function and fluidity (Bento-Oliveira et al., 2020; Hannun and Obeid, 2008; Schlarmann et al., 2021). One
156 of the primary modes of action of sphingolipids is to modulate membrane fluidity, thickness and curvature.
157 In this context, we asked whether there is a direct association of SY1 IBs with certain membrane-bound
158 organelles in the yeast cell. To address this question, we examined the location of SY1 IBs (20 h) in cells
159 and their possible association with membranous organelles visualized by corresponding marker proteins.
160 Our results showed that SY1 IBs had no obvious association with the plasma membrane (Pma1-GFP),
161 vacuole (Vph1-GFP), or ER (Sec63-GFP), but were strongly associated with mitochondria (Tom70-GFP)
162 (Figure 4A and Figure 4-figure supplement 1A, about 80%). Since SY1 IBs have three different
163 morphologies (Class 1-3) and the Class 3 IBs transition to Class 1 during maturation (Figure 1A-C), we
164 wanted to confirm whether all these different IBs associate with mitochondria in a similar way. The results
165 confirmed that all the three different IBs were equivalently associated with mitochondria (Figure 4B and
166 Figure 4-figure supplement 1B). Also, super-resolution microscopy and 3D-SIM techniques demonstrated
167 that the SY1 IBs were surrounded by mitochondria (Figure 4C).

168 The next question is whether other pathogenic IBs are also associated with mitochondria. To address this
169 question, we used the same expression system to overexpress TDP43, FUS1 or Htt103Qp (GFP-labeled) in

170 yeast cells expressing Tom70-RFP and examined the possible association with mitochondria. Our results
171 showed that the IBs of these proteins indeed interacted with mitochondria, similar to what we found for the
172 IBs of SY1 (Figure 4-figure supplement 2). Hence, it appears that the association of IBs with mitochondria
173 may be a common biological event among these disease proteins. To further study the consequences of this
174 association and to decipher potential factors that regulate this association, we first investigated whether SY1
175 IBs physically associate with mitochondria. We performed four co-immunoprecipitation (Co-IP)
176 experiments to determine whether SY1 could be detected in pull-downs for the inner mitochondrial
177 membrane protein Tim44 or the outer mitochondrial membrane proteins Tom70, Tom37, and Sam35. The
178 SY1 protein was indeed the case in extracts obtained from the Tom70-GFP, Tom37-GFP and Tim44-GFP
179 strains (Figure 4D). Next, we performed a microscopic analysis and found that the association of SY1 IBs
180 with mitochondria was significantly hampered in *tom70*Δ*, tom37*Δ and *tim44* mutants (Figure 4E and 4F).
181 Collectively, these results confirm that SY1 IBs are in physical contact with mitochondrial membrane
182 components Tom70, Tom37 and Tim44, which is consistent with the fact that SY1 is a membrane lipid raft
183 interacting protein (Büttner *et al.*, 2010; O'Farrell et al., 2001; Takahashi *et al.*, 2006).

184 **Sphingolipids regulate SY1-induced mitochondrial toxicity in yeast cells**

185 Several lines of evidence have supported the notion that potentially toxic proteins such as α-Syn and TDP-
186 43 can associate with mitochondria and damage the mitochondrial membrane, leading to cytotoxicity
187 (Bäuerlein et al., 2017; Busciglio et al., 2002; Hashimoto et al., 2003; Hsu et al., 2000; Park et al., 2020;
188 Wang et al., 2019a; Wang et al., 2019b). For example, pathogenic α-Syn aggregates preferentially bind to
189 mitochondria, leading to decreased mitochondrial biogenesis (Park *et al*., 2020) and impaired cellular
190 respiration (Wang *et al*., 2019b). To explore whether the interaction between SY1 IBs and mitochondrial
191 membranes could impair mitochondrial function, we measured mitochondrial membrane potential,
192 intracellular ROS levels, and cell viability represented by ATP levels in SY1-expressing cells. The results
193 showed that mitochondrial membrane potential and cell viability of SY1-expressing cells were significantly
194 lower than that of control cells, while ROS levels were increased in SY1 expressing cells (Figure 5A). These
195 changes indicate a decrease in mitochondrial function caused by SY1 IBs. Given that SY1 IBs interact with
196 sphingolipid-enriched membrane raft domains and that sphingolipid metabolism regulates the maturation of
197 SY1 IBs, we wondered whether sphingolipids play a role in the observed SY1-induced mitochondrial
198 dysfunction. To address this question, we first blocked the sphingolipid synthesis by myriocin in the SY1-

199 expressing yeast cells and measured mitochondrial membrane potential, intracellular ROS and cell viability.
200 We found that myriocin treatment aggravated SY-1-induced cytotoxicity, as indicated by decreased
201 mitochondrial membrane potential and cell viability, and increased intracellular ROS (Figure 5B), without
202 altering SY1 protein expression (Figure 5-figure supplement 1A). Second, we added exogenous DHS to
203 SY1-expressing cells and observed ameliorated SY-1-induced cytotoxicity as indicated by increased
204 mitochondrial membrane potential and cell viability, as well as decreased intracellular ROS (Figure 5C),
205 without altering SY1 protein expression (Figure 5-figure supplement 1B). Collectively, these results showed
206 that sphingolipids regulated the mitochondrial toxicity induced by SY1 IBs, and suggested that sphingolipids
207 might detoxify SY1 IBs through mitochondria.

208 **SPTLC2 knockout alters the morphology of SY1 IBs and increases the cytotoxicity in mammalian**
209 **cells**

210 We then wondered whether the observed association with mitochondria and the cytotoxicity of SY1 IBs was
211 conserved in mammalian cells. Similarly, SY1 forms IBs in mammalian cells, which are known as
212 aggresomes (Zaarur et al., 2008). First, we expressed SY1 in HEK293t cells to study the association of SY1
213 IBs with mitochondria. A 3D structure between SY1 IB and mitochondria was constructed by fluorescence
214 3D reconstruction and it confirmed that in these mammalian cells the SY1 IBs are in close contact with
215 mitochondria, although the morphology of the mitochondrion is different (Figure 6A). Furthermore, the
216 mitochondrial membrane potential was significantly decreased in SY1-expressing cells, while the levels of
217 intracellular ROS and mitochondrial superoxide were significantly increased (Figure 6B), indicating
218 impaired mitochondrial function by SY1 IBs. As such, our data suggest that in yeast and mammalian cells
219 the formation and processing of SY1 IBs occur in a similar manner, leading to mitochondrial dysfunction
220 through influencing the mitochondrial membranes.

221 To further confirm this, we analyzed whether sphingolipids are indeed involved in the formation and
222 cytotoxicity of SY1 IBs in mammalian cells as well. To this end, we used the CRISPR/Cas9 approach to
223 knock out SPTLC2, the ortholog of yeast LCB2 and one of the subunits of the mammalian SPT complex
224 (Figure 6-figure supplement 1). Notably, knockout of SPTLC2 significantly reduced the accumulation of
225 intracellular sphingolipids, but had little effect on normal cell division and morphology (Tafesse et al., 2015).
226 Microscopic analysis showed that the morphology of SY1 IBs formed in mammalian cells can be divided
227 into two forms, one compact and spherical and the other more dispersed with an irregular structure as if

228 many small IBs stuck together, without clear boundaries or uniform centers (Figure 6C). In wild-type cells,
229 the SY1 IBs were predominantly spherical. However, in SPTLC2 knockout cells, the morphology of SY1
230 IBs was significantly altered, with an increased number of dispersed irregular IBs (Figure 6D) and an
231 increased number of SY1 IBs per cell (Figure 6-figure supplement 2). This is consistent with the phenotypes
232 observed in SPT mutant yeast cells (Figure 3B). Furthermore, mitochondrial function, as judged from cell
233 viability, intracellular ROS levels and mitochondrial membrane potential, was decreased in the SPTLC2-
234 deficient cells (Figure 6E), while the SY1 protein expression was not altered (Figure 6-figure supplement 3).
235 Taken together, these results further substantiate that SY1 IBs are processed and managed similarly in
236 mammalian cells and in yeast cells and that the sphingolipid pathway plays a role in the cytotoxicity of SY1
237 IBs in mammalian cells as well.

238 **Sphingolipids regulate SY1-induced cytotoxicity and SY1 IB morphology in mammalian cells**

239 Because the initial steps of sphingolipid biosynthesis are conserved from yeast to humans, myriocin also
240 inhibits the de novo synthesis of intracellular sphingolipids in mammalian cells (Ogretmen, 2018). We added
241 myriocin to SY1-expressing HEK293t cells and examined the corresponding changes in cytotoxicity. The
242 results showed that inhibition of the intracellular sphingolipid synthesis pathway by myriocin enhanced SY1
243 cytotoxicity based on ATP content, intracellular ROS and mitochondrial membrane potential assays (Figure
244 7A). Furthermore, the addition of exogenous DHS rescued the cytotoxicity caused by SY1 expression
245 (Figure 7B) without altering SY1 protein expression (Figure 7-figure supplement 1A and B).

246 We further examined the cytotoxicity of SY1 in SPTLC2 knockout cells with or without DHS. The results
247 showed that DHS restored the morphology of IBs (Figure 7C), as well as the number of SY1 IBs formed in
248 SPTLC2 knockout cells (Figure 7-figure supplement 2). Accordingly, DHS also ameliorated the SY1-
249 instigated cytotoxicity by normalizing cell viability, intracellular ROS, and mitochondrial membrane
250 potential (Figure 7D), without affecting SY1 expression (Figure 7-figure supplement 1C). These results
251 reinforce the notion that sphingolipid metabolism plays an important role in the formation of SY1 IBs and
252 SY1-induced cytotoxicity.

253

254 ## Discussion

255 In this study, we used a genome-wide high-content imaging-based screening approach to identify regulators

256 of SY1 IBs formation. Among the 5500 mutants, 84 mutants exhibited increased Class 3 SY1 inclusions.
257 GO enrichment analysis revealed the SPT complex as the most enriched functional group. Subsequent
258 studies revealed that the sphingolipid pathway plays an important role in the processing of SY1 IBs and the
259 detoxification of SY1 by mitochondria in yeast cells. Corresponding experiments in mammalian cells
260 recapitulated the role of sphingolipids in the detoxification of SY1-induced mitochondrial toxicity. Taken
261 together, our results suggest a role for sphingolipids in controlling the cytotoxicity of pathologically
262 aggregated proteins in cells.

263 **IBs management and their cytotoxicity**

264 The formation and accumulation of abnormal intracellular protein aggregates, including the pathological
265 aggregates observed in neurodegenerative diseases, are generally considered to be a double-edged sword.
266 On the one hand, their ability to co-aggregate and sequester basic cellular components, including molecular
267 chaperones, causes cytotoxicity (Gong et al., 2012; Olzscha et al., 2011; Park et al., 2013). On the other hand,
268 formation of protein aggregates can also protect cells against highly toxic, soluble oligomeric substances
269 (Arrasate et al., 2004; Douglas et al., 2008; Tanaka et al., 2004). Many studies have shown that converting
270 small aggregates/oligomers into IBs can reduce the cytotoxicity of various aggregated proteins (Miller et al.,
271 2015). In line with a previous report (Büttner *et al.*, 2010), our current study demonstrated that the merging
272 of smaller foci into IBs also occurred when SY1 was expressed in yeast and mammalian cells.

273 **Association of mitochondrial with protein aggregates**

274 The formation of large intracellular IBs leads to severe impairment of membrane function of IB-bound
275 organelles, thereby affecting organelle function. This has been confirmed in several experiments, such as the
276 disruptive effect of Huntingtin polyQ IBs on ER function (Bäuerlein *et al.*, 2017) and the effect of neuronal
277 *C9orf72* poly-GA aggregates on the Proteasome (Guo et al., 2018). Several lines of evidence implicate
278 mitochondrial dysfunction as a primary cause of PD. Environmental toxins such as mitochondrial complex
279 inhibitors rotenone and 1-methyl-4-phenyl-1,2,3,6-tetrahydropyridine induce dopaminergic neuronal death
280 (Polito et al., 2016). In addition, mitochondrial complex I deficiency and mitochondrial electron transport
281 chain defects have been reported in the nigra of PD patients (Haelterman et al., 2014). However, it is unclear
282 how these protein aggregates affect the mitochondria. As previously reported, small foci formed by SY1
283 started to merge into larger deposits when cells approached the diauxic shift to reprogram metabolism from

284 fermentation to respiration (Büttner *et al.*, 2010), which was confirmed by our present study (Figure 1A). In
285 addition, we show that SY1 physically interacts with mitochondrial membrane proteins and that larger SY1
286 deposits are surrounded by mitochondrial structures in both yeast and mammalian cells (Figure 4A-D and
287 Figure 6A). However, it is unknown why these IBs preferentially interact with mitochondria. This preference
288 may be partly explained by a recent study in which the authors showed that the mitochondrial import receptor
289 Tom70 could nucleate stress-induced aggregation of cytosolic proteins (Liu, 2021). In addition, impaired
290 mitochondria could form cytosolic aggregates and thereby stimulate the aggregation of other proteins,
291 including many pathogenic proteins such as α-Syn and amyloid β (Bento-Oliveira *et al.*, 2020). In this study,
292 however, we did not investigate the influence of mitochondria on SY1 IBs formation. Nevertheless, our
293 current study shows a fine management of aggregated proteins In eukaryotic cells—protein IBs are tightly
294 associated with mitochondria once formed and continue to mature onto mitochondria.

295 In addition to SY1, there is a similar association of IBs and mitochondria with other aggregation-prone
296 proteins, including TDP43, FUS1 and Htt103Qp (Figure 4-figure supplement 2), suggesting that
297 mitochondrion-contact may be a common feature for the maturation of pathogenic protein IBs. Additional
298 experiments are needed to confirm this hypothesis, although an interaction with mitochondria has already
299 been described for the aforementioned and several other aggregation-prone proteins (reviewed in (Abramov
300 et al., 2017)). Furthermore, it would be of great value to illustrate how these IBs are sequestered to
301 mitochondria and how the smaller IBs merge into large IBs with the help of mitochondria.

302 **The role of sphingolipids in SY1 IB maturation and mitochondrial function.**

303 Sphingolipids are structural molecules of cell membranes with important roles in maintaining barrier
304 function and fluidity (Hannun and Obeid, 2008). In addition, bioactive sphingolipids have variety of
305 functions that are involved in almost all major aspects of cell biology, and key sphingolipid metabolites are
306 critical for normal brain development and function (Hannun and Obeid, 2018). Membranes and membrane
307 dynamics are required for these processes and an imbalance of lipids, including ceramide and sphingolipid
308 intermediates, may contribute to mitochondrial dysfunction that could lead to the demise of neurons (Lin et
309 al., 2019). SY1 inclusions co-localize with lipid droplets and endomembranes, and SY1 interacts with
310 cytoplasmic lipid rafts in mammalian cells and yeast (Büttner *et al.*, 2010; Takahashi *et al.*, 2006). The C-
311 terminus of SY1 was found to bind selectively to acidic phospholipids, including phosphatidic acid,
312 phosphatidylserine, and phosphatidylglycerol, but not to naturally charged phospholipids and the amino acid

313 sequence 610-640 was found to represent the major determinant of phospholipid binding (Takahashi *et al.*,
314 2006). The opening question is how sphingolipids contribute to the SY1 IB maturation: do they merely
315 provide a structural basis for docking or do they have an active function in triggering this process. Moreover,
316 the relationship between sphingolipids and mitochondrial function during aging is not fully understood. It
317 has long been appreciated that mitochondrial activity and quality decline with age (reviewed in(Amorim et
318 al., 2022; Lima et al., 2022)). On the other hand, sphingolipids play critical roles in the regulation of lifespan
319 in yeast, worms, and flies, and in the regulation of senescence in mammalian cells (Li and Kim, 2022; Singh
320 and Li, 2018; Trayssac et al., 2018). However, the changes in sphingolipid profiles during aging have not
321 been fully characterized. In mammalian cells, there is an accumulation of ceramide and sphingosine during
322 aging (Sacket et al., 2009), but the levels of other species including long-chain base sphingolipids are not
323 reported. In this regard, additional studies will be needed to profile the sphingolipid species in the aged cells
324 and to identify the major sphingolipids that regulate mitochondrial function.

325

326 Materials and methods

327 Plasmids

328 All plasmids used in this study are listed in Supplementary file 3. The plasmid pYX212-DsRed-SY1-His
329 was constructed by replacing the URA3 cassette with the His3MX6 cassette by homologous recombination
330 in yeast. The corresponding plasmids for complementation experiments were derived from the MoBY library
331 (Ho et al., 2009). The plasmids in this collection were constructed based on the p5472 plasmid with its native
332 promoter and terminator. To construct plasmid pcDNA3.1-GFP-SY1, the GFP fragment and the SY1
333 fragment were inserted into the Not I/Hind III digested pcDNA3.1 (-) vector using Exnase (Vazyme, C112).
334 For the construction of plasmid pcDNA3.1-SY1-Flag, the PCR-expanded SY1-Flag fragment was inserted
335 directly into the Not I/Hind III digested pcDNA3.1 (-) vector.

336 Yeast strains and growth conditions

337 The yeast strains used in this study are listed in Supplemental file 4. Experiments were mainly performed in
338 the BY4741 strain (MATa *his3Δ1 leu2Δ0 met15Δ0 ura3Δ0*) and its respective mutants. The *S. cerevisiae*
339 MATα strain Y7092 (Tong and Boone, 2007) was used for query strain constructions. The yeast single gene
340 knockout collection (SGA-V2) and the essential gene temperature sensitive allele collection (ts-V5) were

341 kindly provided by Prof. Charlie Boone, University of Toronto, Canada. Strains expressing Pma1-GFP,
342 Sec63-GFP, Vph1-GFP, Tom70-GFP, Tom37-GFP, Sam35-GFP, and Tim44-GFP were obtained from the
343 yeast GFP collection (Huh et al., 2003). Yeast strains were grown in YPD (1% yeast extract, 2% peptone,
344 and 2% glucose) or appropriate synthetic drop-out medium (0.17% yeast nitrogen base without amino acids
345 and ammonium sulfate, 0.5% ammonium sulfate and the appropriate synthetic drop-out amino acid, and 2%
346 glucose). Yeast cells were grown at 30°C or at 22°C in case of temperature sensitive (ts) alleles.

347 **SGA analysis**

348 The experimental methods are based on a previous report (Zhao *et al.*, 2016), and essentially consist of
349 transforming the plasmids pYX212-Dsred-SY1 and pYX212-Dsred (control), respectively, into the yeast
350 query strain Y7092. Subsequently, SGA mating was performed as previously described (Tong et al., 2001;
351 Tong et al., 2004) to introduce the plasmids pYX212-Dsred-SY1 or pYX212-Dsred into the SGA-V2 and
352 ts-V5 collections, respectively. All pinning steps for collection handling were performed using a SINGER
353 ROTOR HDA robot (Singer Instrument, Watchet UK).

354 For the genome-wide high content imaging screening of SY1 IB morphology, the constructed collections
355 expressing Dsred-SY1 were pre-cultured in 200 μL SD-Ura liquid medium in 96-well plates with antibiotics
356 at 30°C (22°C for ts mutants) for 3 days without shaking. Then, each pre-culture sample was diluted to
357 OD_{600nm} 0.1 to a final volume of 200 μL of SD-Ura medium. After 20 h (24 h for ts mutants) of incubation
358 with shaking at 30°C (for both single and ts mutants), cells were fixed by adding formaldehyde to a final
359 concentration of 3.7% for 30 min at room temperature and then washed twice with 1×PBS. For imaging,
360 appropriate amounts of fixed cells were transferred to new 96-well glass bottom plates (Matri-plate) with
361 200 μL of 1×PBS in each well and imaged using ImageXpress MICRO (Molecular Devices Corporation
362 (MDC), San Jose, USA), an automated cellular imaging system. To automatically quantify cells with
363 different SY1 aggregation phenotypes, a customized subprogram of the MetaXpress software (MDC) was
364 used (Zhao *et al.*, 2016). Image preprocessing with shading correction and background subtraction was first
365 performed; cells and IBs were separated from their background based on differences in signal intensity,
366 respectively. Then, the number of IBs per cell was extracted by combining the two masks (cell and inclusion
367 body). The percentages of the three types (class 1 to class 3) of cells were counted. All mutants that showed
368 statistically significant differences as compared to the wild-type were re-streaked, individually tested, and
369 further manually analyzed to confirm the phenotypic differences observed in the screen. At least 300 cells

370 were counted for manual confirmation. For manual confirmation, cells were grown from a starting OD_{600nm}
371 of 0.1 in 15 ml Falcon tubes for 20 h (24 h for ts mutants) and fixed and washed as described above. All
372 manual confirmations were verified using a Zeiss Axio Observer 7 microscope (Carl Zeiss, Jena, Germany).

373 **Spot assays**

374 For spot assays, the mutants carrying DsRed-SY1 were cultured in 3 mL SD-Ura liquid medium at 22°C for
375 24 h. The strains were diluted to $OD_{600\ nm}$ = 0.5 and then serially diluted tenfold in sterile water in 96-well
376 plates. The dilutions were spotted on plates with or without DHS. Images were captured after incubation at
377 30°C for 2 days.

378 **Bioinformatic analysis**

379 Candidate hits were analyzed for enrichment in the Gene Ontology (GO) using ClueGO (V2.5.9) (Bindea et
380 al., 2009) in Cytoscape (V3.9.1) with a cut-off of $P < 0.05$. Bubble and network plots of significantly altered
381 GO terms and genes were generated using OmicStudio tools (https://www.omicstudio.cn/tool) and
382 Cytoscape.

383 **Isolation of SY1-expressing old yeast cells**

384 Old yeast cells overexpressing SY1 were obtained by magnetic sorting (Smeal et al., 1996). The wild-type
385 BY4741 cells expressing Dsred-SY1 were cultured in 100 mL SD-Ura liquid medium, and then harvested
386 after growth to 0.5 with an OD_{600nm} of 0.1, washed three times in ice-cold PBS pH7.4, and incubated with 1
387 mg/mL sulfo-NHS-LC biotin (Thermo Scientific, 21335) labeling for 20 min at room temperature. Cells
388 were further washed four times with cold PBS pH 8.0 and grown overnight in 100 mL new fresh medium.
389 Cells were harvested the next day and washed three times with cold PBS pH 7.4, and incubated with 250
390 mL streptavidin-conjugated paramagnetic beads (5 mg/ml, Thermo Scientific, 88817) for 2 h at 4°C.
391 Unlabeled cells were removed by magnetic sorting. The cells were then grown overnight in 100 mL fresh
392 SD-Ura medium. The isolation process was repeated two more times. At the final isolation, cells were
393 collected from the supernatant of the first wash and resuspended in PBS to serve as the young cells, while
394 cells labeled with magnetic beads were centrifuged and resuspended in PBS to serve as old cells. The yeast
395 bud scars were photographed through the DAPI channel using a Zeiss Axio Observer 7 fluorescence
396 microscope to confirm and calculate the degree of yeast senescence. Subsequently, the SY1 aggregates were
397 photographed through the Dsred channel to calculate the type of SY1 aggregates.

398 **Complementation of yeast mutants with MoBY plasmid**

399 The mutants expressing pYX212-DsRed-SY1 were transformed with the corresponding MoBY plasmid or
400 empty control vector (p5472). For the morphological observation experiment of SY1 IBs, the cells were
401 cultured in SD-Ura, His liquid medium at 30ºC starting from OD_{600nm} = 0.1 for 20 h. The cells were then
402 inspected by a fluorescence microscope and photographed.

403 **Myriocin treatment and DHS supplementation in yeast**

404 Myriocin (MCE, HY-N6798) was dissolved in DMSO at a concentration of 10 mM. The stock solution was
405 incubated in a 55°C water bath for 15 min prior to use. DHS (dihydrosphingosine, Sigma, D3314) was
406 prepared in distilled DMSO to 30 mM stock solution. For treatments, cells were grown overnight and diluted
407 in medium to an initial OD_{600nm} of 0.1 with myriocin or DHS at a final concentration of 25 or 20 μM,
408 respectively.

409 **Microscopic analysis of SY1 IBs in yeast**

410 For the microscopic analysis of SY1 IBs in yeast and the co-localization analyses of SY1 IBs with
411 fluorescently labeled proteins Pma1-GFP, Sec63-GFP, Vph1-GFP, and Tom70-GFP, pYX212-DsRed-SY1
412 was transformed into corresponding cells and yeast strains were grown overnight and diluted in culture
413 medium to a starting OD_{600nm} of 0.1. After shaking at 30°C for 20 h, the cells were fixed by adding
414 formaldehyde. Cell images were captured using Zeiss Axio Observer 7. For mitochondrial staining analysis,
415 MitoTracker Green (Invitrogen, M7514) staining solution was prepared according to the manufacturer's
416 protocol. After 20 h of growth from an OD_{600nm} of 0.1, 1×10^7 cells were fixed with formaldehyde for 30 min
417 and then washed twice in 1×PBS (pH 7.4). The cells were resuspended in 1× PBS (pH 7.4) containing 125
418 nM MitoTracker probe and incubated for 30 min at room temperature. After one wash with PBS, the cells
419 were imaged by microscopy.

420 **3D-SIM microscopy**

421 3D-SIM microscopy images were obtained as previously reported (Song et al., 2014). Briefly, yeast strain
422 Tom70-GFP expressing pYX212-DsRed-SY1 was grown overnight and diluted in medium to a starting
423 OD_{600nm} of 0.1. After shaking at 30°C for 20 h, cells were fixed with 3.7% formaldehyde and washed twice
424 with 1× PBS (pH 7.4). The ELYRA PS.1 LSM780 setup from Zeiss (Carl Zeiss, Jena, Germany) was used

425 for 3D-SIM. Images were acquired with a 100×/1.46 Plan-Apochromat oil immersion objective. Z-stacks
426 with 100 nm spacing were used to scan the whole yeast in 3D-SIM. Zeiss Zen microscope software was used
427 for acquisition, super-resolution processing and calculation, and 3D reconstruction. The ELYRA system was
428 corrected for chromatic aberration in x-, y- and z-directions using multi-color beads, and all obtained images
429 were inspected and aligned accordingly.

430 **Co-IP for SY1 with mitochondrial membrane proteins in yeast**

431 pYX212-DsRed-SY1 and pYX212-DsRed were transformed into GFP strains (Tom70-GFP, Tom37-GFP,
432 Sam35-GFP, and Tim44-GFP) respectively. The strains were pre-cultured and diluted to 100 mL medium
433 with OD_{600nm}=0.1. Cells were harvested when OD_{600nm} reached 1.0 by centrifugation at 4000 rpm for 5 min
434 at 4°C and washed twice with 20 mL ice-cold ddH_2O water. Cells were then washed with 1 mL ice-cold IP
435 buffer (115 mM KCl, 5 mM NaCl, 2 mM $MgCl_2$, 1 mM EDTA, 20 mM HEPES/KOH, pH 7.5), and
436 transferred to 1.5 mL Eppendorf tubes. Cell pellets were resuspended in 250 μL IP buffer containing protease
437 inhibitors, DTT, and glass beads and disrupted using a FastPrep-24 device (MP Biomedicals). Cells were
438 further lysed on ice for 20 min with additional IP buffer containing 0.5% Nonidet P-40 (NP-40, Beyotime,
439 ST2045). The lysates were centrifuged at 16,000 g for 20 min at 4°C, and 700-800 μL of supernatant was
440 transferred to a new tube. For the IP assay, 20 μL anti-GFP beads (chromoTek, GFP-Trap) were resuspended
441 in 100 μL IP buffer and mixed with the supernatant. The mixture was incubated for 1-1.5 h at 4°C on an
442 overhead rotator, centrifuged at 2000 rpm for 1 min, and washed 4 times with 1 mL IP buffer containing 0.5%
443 NP-40. The final eluted proteins were boiled with 2 x Laemmli buffer / 5% beta-mercaptoethanol for 10 min
444 at 95°C and the supernatant was used for Western blot analysis.

445 **Detection of ROS and mitochondrial membrane potential in yeast cells**

446 To examine ROS levels and mitochondrial membrane potential in yeast cells, BY4741 yeast cells expressing
447 pYX212-DsRed-SY1 or pYX212-DsRed were pre-cultured overnight and diluted to an OD_{600nm} of 0.1. Cells
448 were harvested at the endpoints, washed twice with 1× PBS (pH 7.4), and treated with DCFH-DA (Beyotime,
449 S0033S) or Rhodamine123 (Beyotime, C2007) at a final concentration of 10 μM. Cells were incubated for
450 20 min at 30°C in the dark. Cells were then washed at least three times with 1×PBS (pH 7.4) before flow
451 cytometric analysis using BD Accuri C6 (BD Biosciences, San Jose, USA) with FITC channel.

452 **Cell lines, culture condition, transfection and drug treatment**

453 The human embryonic kidney (HEK293t) cell line was obtained from the National Collection of
454 Authenticated Cell Cultures (NCACC; Shanghai, China). Cells were cultured in Dulbecco's modified Eagle's
455 medium (DMEM; Gibco, c11995500bt) supplemented with 10% fetal bovine serum (FBS; Biological
456 Industries, 04-001-1acs) and 1% penicillin-streptomycin (HycloneTM, SV30010) in a humidified incubator
457 containing 5% CO_2 at 37°C. Transfection was performed on six-well plates or confocal dishes for different
458 purposes with plasmids using X-tremeGENE HP DNA Transfection Reagent (Roche, 6366236001)
459 according to the manufacturer's protocol. For drug treatment, cells were seeded at appropriate density in cell
460 culture plates and cultured for 24 h. Cells were treated with 25 μM myriocin for 3 days or 20 μM DHS for 2
461 days before subsequent analysis.

462 **Cell imaging in mammalian cells**

463 To observe the association of SY1 IBs with mitochondria in mammalian cells, HEK293t cells were seeded
464 into 35 mm confocal cell culture dishes (BioSharp), transfected with GFP-SY1, and incubated for 24 h. The
465 cells were washed with PBS and then stained with 10 μM MitoTracker Deep Red FM (Invitrogen, M22426)
466 at 37°C for 20 min. After staining, the cells were washed twice with PBS, and rinsed with PBS. Fluorescence
467 images were captured using a Zeiss LSM 880 confocal microscope (Carl Zeiss, Jena, Germany), and Z-stack
468 images for 3D rendering were taken at 0.4 μm interlayer distance. 3D rendering was performed using the
469 Surface tool in the Imaris software (version 9.0.1; Bitplane AG).

470 For analysis of SY1 IBs formation under myriocin or DHS treatment, HEK293t cells were seeded in confocal
471 culture dishes and transfected with pcDNA3.1-GFP-SY1 after treatment. Cells were fixed with 4%
472 paraformaldehyde (Beyotime, P0099) for 20 min and permeabilized with 0.1% (v/v) Triton X-100 in PBS
473 (Beyotime, P0096) for 15 min on ice. The cytoskeleton was then stained with phalloidin-Atto 565 (Sigma,
474 94072), followed by nuclei with DAPI (Southern Biotech, 0100-20). Images were captured using a Zeiss
475 LSM 880 confocal microscope.

476 **Measurement of mitochondrial function in mammalian cells**

477 HEK293t cells were detached and transferred to 75-mm flow tubes and exposed to 5 μM MitoSOX
478 (Invitrogen, M36008) or 10 μM DCFH-DA (Beyotime, S0033S) in serum-free medium for 10 min
479 (MitoSOX) or 20 min (DCFH-DA) in a 37°C cell incubator. Cells were then washed three times with serum-
480 free cell culture medium and analyzed using a BD Accuri C6 flow cytometer.

481 Mitochondrial membrane potential (MMP) was measured with JC-1 (Beyotime, C2006) according to the
482 manufacturer's instructions. Briefly, treated cells were harvested, washed twice with PBS, and then stained
483 in a mixture of 500 μL medium and 500 μL JC-1 at 37°C for 20 min in the dark. Cells were washed 3 times
484 with staining buffer and analyzed by flow cytometry. Changes in MMP are represented by the ratio of red to
485 green fluorescence intensity.

486 **Measurement of cell viability and cytotoxicity**

487 Cell viability was measured by monitoring the cellular ATP content using a CellTiter-Lumi Luminescent
488 Cell Viability Assay Kit (Beyotime, C0065S). Cells were treated and further incubated with 100 μL of
489 detection reagent at room temperature for 2 min to promote cell lysis. Cells were further incubated at room
490 temperature for 10 min to stabilize the luminescence signal, and ATP levels were then analyzed by using a
491 Spark multimode microplate reader (Tecan Trading AG, Männedorf, Switzerland).

492 **Western blot analysis**

493 Cells were harvested and lysed in RIPA buffer (Beyotime, P0013C) supplemented with a protease inhibitor
494 of 1 mM PMSF (Beyotime, ST506). Total protein concentrations were then quantified using the BCA Protein
495 Quantification Kit (Beyotime, P0012S). A total of 20 μg of protein from each sample was separated by SDS-
496 PAGE and transferred to nitrocellulose membranes (Cytiva, 10600001). The membranes were blocked with
497 1% BSA for 1 h at 37°C and incubated with primary antibodies: anti-Flag (Cell Signaling, D6W5B, 1:1000
498 dilution), anti-GFP (Abcam, ab6556, 1:1000 dilution), anti-SY1 (Affinity, DF8619, 1:1000 dilution), anti-
499 PGK1 (Abcam, ab113687, 1:1000 dilution), anti-GAPDH (Wanleibio, WL01114, 1:1000 dilution), followed
500 by HRP-conjugated secondary antibody incubation: goat anti-rabbit IgG (Abcam, ab6721, 1:10000 dilution).
501 Protein bands were detected with ECL Prime Western Blotting Detection Reagent (GE, RPN2232) using an
502 Amersham imager 600 (GE, Piscataway, USA).

503 **Generation of HEK293t SPTLC2 knockout cells by CRISPR/Cas9**

504 For the generation of SPTLC2 knockout cell line, guide RNA sequences for CRISPR were designed at
505 CRISPR design web site (http://crispr.mit.edu/). Guide RNA sequences for human SPTLC2 were #1: 5'-
506 CGAATGGCTGCGTGGCGAAC-3' and #2: 5'-AAGTACGGAACGGGTACGTG-3', respectively. Both
507 guide RNAs target the exon 1 of the SPTLC2 gene (Figure 6-figure supplement 1). The DNA sequence of
508 the guide RNA (gRNA) was synthesized and cloned into the pX459 CRISPR/Cas9-Puro vector to construct

knockout plasmids px459-SPTLC2-gRNA1 and px459-SPTLC2-gRNA2.

Cells were seeded at appropriate densities in 35-mm dishes and grown for 24 h before transfection with the plasmids. 48 h after transfection, cells were treated with 2 μg/mL Puromycin (Sangon Biotech, A610593) for an additional three days. Single cells were then obtained by serial dilution and cultured for expansion. Genomic DNA was extracted from 18 single-cell expansion cultures and primers 5'-GCCACCGCCTACAGAGCCTGC-3' / 5'-CCGGGAGTAAGACCTCCAGGCGC-3' were used to amplify the exon 1 sequence of SPTLC2 by PCR. Two cell lines with deletion mutations were identified by sequencing (Figure 6-figure supplement 1).

Statistical analysis

Three or more biological replicates were analyzed unless explicitly stated. Statistical significance was indicated as $p < 0.05$ unless explicitly stated. All graphs show mean and error bars representing standard error of the deviation (S.D.), using Prism 8.0.0 software (GraphPad Software).

Acknowledgments

We would like to thank Professor Charles Boone (University of Toronto) for providing SGA-V2 and ts-V5 strain collections, as well as the Moby plasmids. We also thank the Centre for Cellular Imaging at University of Gothenburg for microscopy support, and Center for Large-scale cell-based screening at University of Gothenburg for assistance with SGA analysis.

Additional information

Funding

Funder	Grant reference number	Author
National Natural Science Foundation of China	32000387	Xiuling Cao
Zhejiang Provincial Natural Science Foundation of China	LY23C060001	Xuejiao Jin
Scientific Research Foundation of Zhejiang A&F University	2021LFR053	Xuejiao Jin

Fellowship from China Scholarship Council and KU Leuven	grant C14/17/063	Ju Zheng
Swedish Cancer Fund (Cancerfonden)	19 0069	Beidong Liu
Swedish Research Council (Vetenskapsrådet)	VR 2019-03604	Beidong Liu
Guangdong Basic and Applied Basic Research Foundation	2023A1515010483	Lihua Chen
FWO-Vlaanderen	G0C7222N	Joris Winderickx
KU Leuven	C14/21/095	Joris Winderickx
The funders had no role in study design, data collection and interpretation, or the decision to submit the work for publication.		

Author contributions

Conceptualization: Beidong Liu; Methodology: Xiang Wu, Lei Zhao., Ju Zheng, Xinxin Hao; Investigation: Xiuling Cao, Lei Zhao, Xuejiao Jin, Lihua Chen, Beidong Liu; Visualization: Xiuling Cao, Xiang Wu, Lei Zhao, Lihua Chen. Supervision: Xiuling Cao, Shenkui Liu, Lihua Chen, Beidong Liu; Writing—original draft: Xiuling Cao, Lei Zhao, Lihua Chen; Writing—review & editing: Xiuling Cao, Joris Winderickx, Lihua Chen, Beidong Liu.

Additional files

Supplementary files

Supplementary file 1. Mutants with manually confirmed increased class 3 synphilin-1 aggregates.

Supplementary file 2. Distribution of GO terms among 84 candidate hits with significantly increased Class 3 aggregates via ClueGO analysis.

Supplementary file 3. Plasmids used in this study.

Supplementary file 4. Strains used in this study.

Data availability

All data generated or analyzed during this study are included in the manuscript and supplementary information. No datasets have been submitted to public repositories.

548 **References**

549 Abramov, AY, Berezhnov, AV, Fedotova, EI, Zinchenko, VP, and Dolgacheva, LP. 2017. Interaction of misfolded
550 proteins and mitochondria in neurodegenerative disorders. *Biochemical Society Transactions* **45**: 1025-1033.
551 https://doi.org/10.1042/bst20170024

552 Amorim, JA, Coppotelli, G, Rolo, AP, Palmeira, CM, Ross, JM, and Sinclair, DA. 2022. Mitochondrial and
553 metabolic dysfunction in ageing and age-related diseases. *Nature Reviews Endocrinology* **18**: 243-258.
554 https://doi.org/10.1038/s41574-021-00626-7

555 Arrasate, M, Mitra, S, Schweitzer, ES, Segal, MR, and Finkbeiner, S. 2004. Inclusion body formation reduces
556 levels of mutant huntingtin and the risk of neuronal death. *Nature* **431**: 805-810.
557 https://doi.org/10.1038/nature02998

558 Bagola, K, and Sommer, T. 2008. Protein quality control: on IPODs and other JUNQ. *Current Biology* **18**: R1019-
559 R1021. https://doi.org/10.1016/j.cub.2008.09.036

560 Bäuerlein, FJB, Saha, I, Mishra, A, Kalemanov, M, Martínez-Sánchez, A, Klein, R, Dudanova, I, Hipp, MS, Hartl,
561 FU, Baumeister, W, and Fernández-Busnadiego, R. 2017. In situ architecture andcellular interactions of PolyQ
562 inclusions. *Cell* **171**: 179-187.e110. https://doi.org/10.1016/j.cell.2017.08.009

563 Bento-Oliveira, A, Santos, FC, Marquês, JT, Paulo, PMR, Korte, T, Herrmann, A, Marinho, HS, and de Almeida,
564 RFM. 2020. Yeast sphingolipid-enriched domains and membrane compartments in the absence of
565 mannosyldiinositolphosphorylceramide. *Biomolecules* **10**: 871. https://doi.org/10.3390/biom10060871

566 Bindea, G, Mlecnik, B, Hackl, H, Charoentong, P, Tosolini, M, Kirilovsky, A, Fridman, WH, Pagès, F, Trajanoski,
567 Z, and Galon, J. 2009. ClueGO: a Cytoscape plug-in to decipher functionally grouped gene ontology and pathway
568 annotation networks. *Bioinformatics* **25**: 1091-1093. https://doi.org/10.1093/bioinformatics/btp101

569 Buchberger, A, Bukau, B, and Sommer, T. 2010. Protein quality control in the cytosol and the endoplasmic
570 reticulum: brothers in arms. *Molecular Cell* **40**: 238-252. https://doi.org/10.1016/j.molcel.2010.10.001

571 Busciglio, J, Pelsman, A, Wong, C, Pigino, G, Yuan, M, Mori, H, and Yankner, BA. 2002. Altered metabolism of
572 the amyloid β precursor protein is associated with mitochondrial dysfunction in Down's Syndrome. *Neuron* **33**:
573 677-688. https://doi.org/10.1016/S0896-6273(02)00604-9

574 Büttner, S, Delay, C, Franssens, V, Bammens, T, Ruli, D, Zaunschirm, S, de Oliveira, RM, Outeiro, TF, Madeo, F,
575 Buée, L, et al. 2010. Synphilin-1 enhances α-synuclein aggregation in yeast and contributes to cellular stress and
576 cell death in a Sir2-dependent manner. *PLoS One* **5**: e13700. https://doi.org/10.1371/journal.pone.0013700

577 Casadei, N, Pöhler, AM, Tomás-Zapico, C, Torres-Peraza, J, Schwedhelm, I, Witz, A, Zamolo, I, De Heer, R,
578 Spruijt, B, Noldus, LP, et al. 2014. Overexpression of synphilin-1 promotes clearance of soluble and misfolded
579 alpha-synuclein without restoring the motor phenotype in aged A30P transgenic mice. *Human Molecular Genetics*
580 **23**: 767-781. https://doi.org/10.1093/hmg/ddt467

581 Chen, B, Retzlaff, M, Roos, T, and Frydman, J. 2011. Cellular strategies of protein quality control. *Cold Spring*
582 *Harbor perspectives in biology* **3**: a004374. https://doi.org/10.1101/cshperspect.a004374

583 Cutler, RG, Pedersen, WA, Camandola, S, Rothstein, JD, and Mattson, MP. 2002. Evidence that accumulation of
584 ceramides and cholesterol esters mediates oxidative stress–induced death of motor neurons in amyotrophic lateral

585 sclerosis. *Annals of Neurology* **52**: 448-457. https://doi.org/10.1002/ana.10312

586 Douglas, PM, Treusch, S, Ren, H-Y, Halfmann, R, Duennwald, ML, Lindquist, S, and Cyr, DM. 2008. Chaperone-
587 dependent amyloid assembly protects cells from prion toxicity. *Proceedings of the National Academy of Sciences,*
588 *USA* **105**: 7206-7211. https://doi.org/10.1073/pnas.0802593105

589 France-Lanord, V, Brugg, B, Michel, PP, Agid, Y, and Ruberg, M. 1997. Mitochondrial free radical signal in
590 ceramide-dependent apoptosis: a putative mechanism for neuronal death in Parkinson's disease. *Journal of*
591 *Neurochemistry* **69**: 1612-1621. https://doi.org/10.1046/j.1471-4159.1997.69041612.x

592 Frydman, J. 2001. Folding of newly translated proteins in vivo: the role of molecular chaperones. *Annual Review*
593 *of Biochemistry* **70**: 603-647. https://doi.org/10.1146/annurev.biochem.70.1.603

594 Gong, H, Romanova, NV, Allen, KD, Chandramowlishwaran, P, Gokhale, K, Newnam, GP, Mieczkowski, P,
595 Sherman, MY, and Chernoff, YO. 2012. Polyglutamine toxicity is controlled by prion composition and gene
596 dosage in yeast. *PLoS Genetics* **8**: e1002634. https://doi.org/10.1371/journal.pgen.1002634

597 Guo, Q, Lehmer, C, Martínez-Sánchez, A, Rudack, T, Beck, F, Hartmann, H, Pérez-Berlanga, M, Frottin, F, Hipp,
598 MS, Hartl, FU, et al. 2018. In situ structure of neuronal C9orf72 Poly-GA aggregates reveals proteasome
599 recruitment. *Cell* **172**: 696-705.e612. https://doi.org/10.1016/j.cell.2017.12.030

600 Haelterman, NA, Yoon, WH, Sandoval, H, Jaiswal, M, Shulman, JM, and Bellen, HJ. 2014. A mitocentric view
601 of Parkinson's disease. *Annual Review of Neuroscience* **37**: 137-159. https://doi.org/10.1146/annurev-neuro-
602 071013-014317

603 Hannun, YA, and Obeid, LM. 2008. Principles of bioactive lipid signalling: lessons from sphingolipids. *Nat Rev*
604 *Mol Cell Biol* **9**: 139-150. https://doi.org/10.1038/nrm2329

605 Hannun, YA, and Obeid, LM. 2018. Sphingolipids and their metabolism in physiology and disease. *Nature*
606 *Reviews Molecular Cell Biology* **19**: 175-191. https://doi.org/10.1038/nrm.2017.107

607 Hartl, FU, and Hayer-Hartl, M. 2009. Converging concepts of protein folding in vitro and in vivo. *Nature*
608 *Structural & Molecular Biology* **16**: 574. https://doi.org/10.1038/nsmb.1591

609 Hashimoto, M, Rockenstein, E, Crews, L, and Masliah, E. 2003. Role of protein aggregation in mitochondrial
610 dysfunction and neurodegeneration in Alzheimer's and Parkinson's diseases. *Neuromolecular Medicine* **4**: 21-36.
611 https://doi.org/10.1385/nmm:4:1-2:21

612 Ho, CH, Magtanong, L, Barker, SL, Gresham, D, Nishimura, S, Natarajan, P, Koh, JLY, Porter, J, Gray, CA,
613 Andersen, RJ, et al. 2009. A molecular barcoded yeast ORF library enables mode-of-action analysis of bioactive
614 compounds. *Nature Biotechnology* **27**: 369-377. https://doi.org/10.1038/nbt.1534

615 Hsu, LJ, Sagara, Y, Arroyo, A, Rockenstein, E, Sisk, A, Mallory, M, Wong, J, Takenouchi, T, Hashimoto, M, and
616 Masliah, E. 2000. α-Synuclein promotes mitochondrial deficit and oxidative stress. *The American Journal of*
617 *Pathology* **157**: 401-410. https://doi.org/10.1016/S0002-9440(10)64553-1

618 Huh, WK, Falvo, JV, Gerke, LC, Carroll, AS, Howson, RW, Weissman, JS, and O'Shea, EK. 2003. Global analysis
619 of protein localization in budding yeast. *Nature* **425**: 686-691. https://doi.org/10.1038/nature02026

620 Jin, HG, Yamashita, H, Nakamura, T, Fukuba, H, Takahashi, T, Hiji, M, Kohriyama, T, and Matsumoto, M. 2008.
621 Synphilin-1 transgenic mice exhibit mild motor impairments. *Neuroscience Letters* **445**: 12-17.

https://doi.org/10.1016/j.neulet.2008.08.073

Kaganovich, D, Kopito, R, and Frydman, J. 2008. Misfolded proteins partition between two distinct quality control compartments. *Nature* **454**: 1088-1095. https://doi.org/10.1038/nature07195

Kitamura, A, Kubota, H, Pack, CG, Matsumoto, G, Hirayama, S, Takahashi, Y, Kimura, H, Kinjo, M, Morimoto, RI, and Nagata, K. 2006. Cytosolic chaperonin prevents polyglutamine toxicity with altering the aggregation state. *Nature Cell Biology* **8**: 1163-1170. https://doi.org/10.1038/ncb1478

Kopito, RR. 2000. Aggresomes, inclusion bodies and protein aggregation. *Trends in Cell Biology* **10**: 524-530. https://doi.org/10.1016/S0962-8924(00)01852-3

Krenz, A, Falkenburger, BH, Gerhardt, E, Drinkut, A, and Schulz, JB. 2009. Aggregate formation and toxicity by wild-type and R621C synphilin-1 in the nigrostriatal system of mice using adenoviral vectors. *Journal of Neurochemistry* **108**: 139-146. https://doi.org/10.1111/j.1471-4159.2008.05755.x

Li, S, and Kim, H-E. 2022. Implications of sphingolipids on aging and age-related diseases. *Frontiers in aging* **2**: 797320. https://doi.org/10.3389/fragi.2021.797320

Lim, J, and Yue, Z. 2015. Neuronal aggregates: formation, clearance, and spreading. *Developmental Cell* **32**: 491-501. https://doi.org/10.1016/j.devcel.2015.02.002

Lima, T, Li, TY, Mottis, A, and Auwerx, J. 2022. Pleiotropic effects of mitochondria in aging. *Nature Aging* **2**: 199-213. https://doi.org/10.1038/s43587-022-00191-2

Lin, G, Wang, L, Marcogliese, PC, and Bellen, HJ. 2019. Sphingolipids in the pathogenesis of Parkinson's disease and Parkinsonism. *Trends in Endocrinology and Metabolism* **30**: 106-117. https://doi.org/10.1016/j.tem.2018.11.003

Liu, J, Li, T, Thomas, JM, Pei, Z, Jiang, H, Engelender, S, Ross, CA, and Smith, WW. 2016. Synphilin-1 attenuates mutant LRRK2-induced neurodegeneration in Parkinson's disease models. *Human Molecular Genetics* **25**: 672-680. https://doi.org/10.1093/hmg/ddv504

Liu, QaF, Benjamin and Unruh, Jay R. and Guo, Fengli and Si, Kausik and Li, Rong and Zhou, Chuankai. 2021. Mitochondrial origin of cytosolic protein aggregation. *SSRN* **37**: 3808300. https://doi.org/10.2139/ssrn.3808300

Mielke, MM, and Lyketsos, CG. 2010. Alterations of the sphingolipid pathway in Alzheimer's disease: new biomarkers and treatment targets? *Neuromolecular Medicine* **12**: 331-340. https://doi.org/10.1007/s12017-010-8121-y

Miller, SB, Mogk, A, and Bukau, B. 2015. Spatially organized aggregation of misfolded proteins as cellular stress defense strategy. *Journal of Molecular Biology* **427**: 1564-1574. https://doi.org/10.1016/j.jmb.2015.02.006

Moldavski, O, Amen, T, Levin-Zaidman, S, Eisenstein, M, Rogachev, I, Brandis, A, Kaganovich, D, and Schuldiner, M. 2015. Lipid droplets are essential for efficient clearance of cytosolic inclusion bodies. *Developmental Cell* **33**: 603-610. https://doi.org/10.1016/j.devcel.2015.04.015

Nuber, S, Franck, T, Wolburg, H, Schumann, U, Casadei, N, Fischer, K, Calaminus, C, Pichler, BJ, Chanarat, S, Teismann, P, et al. 2010. Transgenic overexpression of the alpha-synuclein interacting protein synphilin-1 leads to behavioral and neuropathological alterations in mice. *Neurogenetics* **11**: 107-120. https://doi.org/10.1007/s10048-009-0212-2

659 O'Farrell, C, Murphy, DD, Petrucelli, L, Singleton, AB, Hussey, J, Farrer, M, Hardy, J, Dickson, DW, and Cookson,
660 MR. 2001. Transfected synphilin-1 forms cytoplasmic inclusions in HEK293 cells. *Brain Res Mol Brain Res* **97**:
661 94-102. https://doi.org/10.1016/s0169-328x(01)00292-3

662 Ogretmen, B. 2018. Sphingolipid metabolism in cancer signalling and therapy. *Nature Reviews: Cancer* **18**: 33-
663 50. https://doi.org/10.1038/nrc.2017.96

664 Ogrodnik, M, Salmonowicz, H, Brown, R, Turkowska, J, Średniawa, W, Pattabiraman, S, Amen, T, Abraham, A-
665 c, Eichler, N, Lyakhovetsky, R, and Kaganovich, D. 2014. Dynamic JUNQ inclusion bodies are asymmetrically
666 inherited in mammalian cell lines through the asymmetric partitioning of vimentin. *Proceedings of the National*
667 *Academy of Sciences, USA* **111**: 8049-8054. https://doi.org/10.1073/pnas.1324035111

668 Olzscha, H, Schermann, SM, Woerner, AC, Pinkert, S, Hecht, MH, Tartaglia, GG, Vendruscolo, M, Hayer-Hartl,
669 M, Hartl, FU, and Vabulas, RM. 2011. Amyloid-like aggregates sequester numerous metastable proteins with
670 essential cellular functions. *Cell* **144**: 67-78. https://doi.org/10.1016/j.cell.2010.11.050

671 Park, JH, Burgess, JD, Faroqi, AH, DeMeo, NN, Fiesel, FC, Springer, W, Delenclos, M, and McLean, PJ. 2020.
672 Alpha-synuclein-induced mitochondrial dysfunction is mediated via a sirtuin 3-dependent pathway. *Molecular*
673 *neurodegeneration* **15**: 5. https://doi.org/10.1186/s13024-019-0349-x

674 Park, S-H, Kukushkin, Y, Gupta, R, Chen, T, Konagai, A, Hipp, Mark S, Hayer-Hartl, M, and Hartl, FU. 2013.
675 PolyQ proteins interfere with nuclear degradation of cytosolic proteins by sequestering the Sis1p chaperone. *Cell*
676 **154**: 134-145. https://doi.org/10.1016/j.cell.2013.06.003

677 Polito, L, Greco, A, and Seripa, D. 2016. Genetic profile, environmental exposure, and their interaction in
678 Parkinson's Disease. *Parkinson's Disease* **2016**: 6465793. https://doi.org/10.1155/2016/6465793

679 Ribeiro, CS, Carneiro, K, Ross, CA, Menezes, JRL, and Engelender, S. 2002. Synphilin-1 is developmentally
680 localized to synaptic terminals, and its association with synaptic vesicles is modulated by alpha-synuclein. *Journal*
681 *of Biological Chemistry* **277**: 23927-23933. https://doi.org/10.1074/jbc.M201115200

682 Ross, CA, and Poirier, MA. 2004. Protein aggregation and neurodegenerative disease. *Nature Medicine* **10**: S10-
683 17. https://doi.org/10.1038/nm1066

684 Sacket, SJ, Chung, H-y, Okajima, F, and Im, D-s. 2009. Increase in sphingolipid catabolic enzyme activity during
685 aging. *Acta Pharmacologica Sinica* **30**: 1454-1461. https://doi.org/10.1038/aps.2009.136

686 Schlarmann, P, Ikeda, A, and Funato, K. 2021. Membrane contact sites in yeast: control hubs of sphingolipid
687 homeostasis. *Membranes* **11**: 971. https://doi.org/10.3390/membranes11120971

688 Shishido, T, Nagano, Y, Araki, M, Kurashige, T, Obayashi, H, Nakamura, T, Takahashi, T, Matsumoto, M, and
689 Maruyama, H. 2019. Synphilin-1 has neuroprotective effects on MPP(+)-induced Parkinson's disease model cells
690 by inhibiting ROS production and apoptosis. *Neuroscience Letters* **690**: 145-150.
691 https://doi.org/10.1016/j.neulet.2018.10.020

692 Singh, P, and Li, R. 2018. Emerging roles for sphingolipids in cellular aging. *Current Genetics* **64**: 761-767.
693 https://doi.org/10.1007/s00294-017-0799-z

694 Smeal, T, Claus, J, Kennedy, B, Cole, F, and Guarente, L. 1996. Loss of transcriptional silencing causes sterility
695 in old mother cells of *S. cerevisiae*. *Cell* **84**: 633-642. https://doi.org/10.1016/s0092-8674(00)81038-7

696 Smith, WW, Liu, Z, Liang, Y, Masuda, N, Swing, DA, Jenkins, NA, Copeland, NG, Troncoso, JC, Pletnikov, M,
697 Dawson, TM, et al. 2010. Synphilin-1 attenuates neuronal degeneration in the A53T alpha-synuclein transgenic
698 mouse model. *Human Molecular Genetics* **19**: 2087-2098. https://doi.org/10.1093/hmg/ddq086

699 Song, J, Yang, Q, Yang, J, Larsson, L, Hao, X, Zhu, X, Malmgren-Hill, S, Cvijovic, M, Fernandez-Rodriguez, J,
700 Grantham, J, et al. 2014. Essential genetic interactors of SIR2 required for spatial sequestration and asymmetrical
701 inheritance of protein aggregates. *PLoS Genetics* **10**: e1004539. https://doi.org/10.1371/journal.pgen.1004539

702 Tafesse, FG, Rashidfarrokhi, A, Schmidt, FI, Freinkman, E, Dougan, S, Dougan, M, Esteban, A, Maruyama, T,
703 Strijbis, K, and Ploegh, HL. 2015. Disruption of sphingolipid biosynthesis blocks phagocytosis of *Candida*
704 *albicans*. *PLoS Pathogens* **11**: e1005188. https://doi.org/10.1371/journal.ppat.1005188

705 Takahashi, T, Yamashita, H, Nagano, Y, Nakamura, T, Kohriyama, T, and Matsumoto, M. 2006. Interactions of
706 Synphilin-1 with phospholipids and lipid membranes. *FEBS Letters* **580**: 4479-4484.
707 https://doi.org/10.1016/j.febslet.2006.07.019

708 Tanaka, M, Kim, YM, Lee, G, Junn, E, Iwatsubo, T, and Mouradian, MM. 2004. Aggresomes formed by alpha-
709 synuclein and synphilin-1 are cytoprotective. *Journal of Biological Chemistry* **279**: 4625-4631.
710 https://doi.org/10.1074/jbc.M310994200

711 Tong, AH, Evangelista, M, Parsons, AB, Xu, H, Bader, GD, Pagé, N, Robinson, M, Raghibizadeh, S, Hogue, CW,
712 Bussey, H, et al. 2001. Systematic genetic analysis with ordered arrays of yeast deletion mutants. *Science* **294**:
713 2364-2368. https://doi.org/10.1126/science.1065810

714 Tong, AH, Lesage, G, Bader, GD, Ding, H, Xu, H, Xin, X, Young, J, Berriz, GF, Brost, RL, Chang, M, et al. 2004.
715 Global mapping of the yeast genetic interaction network. *Science* **303**: 808-813.
716 https://doi.org/10.1126/science.1091317

717 Tong, AHY, and Boone, C (2007). 16 High-throughput strain construction and systematic synthetic lethal
718 screening in *Saccharomyce scerevisiae*. In Methods in Microbiology, I. Stansfield, and M.J.R. Stark, eds.
719 (Academic Press), pp. 369-707. https://doi.org/10.1016/S0580-9517(06)36016-3

720 Trayssac, M, Hannun, YA, and Obeid, LM. 2018. Role of sphingolipids in senescence: implication in aging and
721 age-related diseases. *Journal of Clinical Investigation* **128**: 2702-2712. https://doi.org/10.1172/jci97949

722 Wang, P, Deng, J, Dong, J, Liu, J, Bigio, EH, Mesulam, M, Wang, T, Sun, L, Wang, L, Lee, AY, et al. 2019a. TDP-
723 43 induces mitochondrial damage and activates the mitochondrial unfolded protein response. *PLoS Genetics* **15**:
724 e1007947. https://doi.org/10.1371/journal.pgen.1007947

725 Wang, X, Becker, K, Levine, N, Zhang, M, Lieberman, AP, Moore, DJ, and Ma, J. 2019b. Pathogenic alpha-
726 synuclein aggregates preferentially bind to mitochondria and affect cellular respiration. *Acta neuropathologica*
727 *communications* **7**: 41. https://doi.org/10.1186/s40478-019-0696-4

728 Weisberg, SJ, Lyakhovetsky, R, Werdiger, A-c, Gitler, AD, Soen, Y, and Kaganovich, D. 2012.
729 Compartmentalization of superoxide dismutase 1 (SOD1G93A) aggregates determines their toxicity. *Proceedings*
730 *of the National Academy of Sciences, USA* **109**: 15811-15816. https://doi.org/10.1073/pnas.1205829109

731 Yang, J, Hao, X, Cao, X, Liu, B, and Nyström, T. 2016. Spatial sequestration and detoxification of Huntingtin by
732 the ribosome quality control complex. *eLife* **5**: e11792. https://doi.org/10.7554/eLife.11792

733 Zaarur, N, Meriin, AB, Gabai, VL, and Sherman, MY. 2008. Triggering aggresome formation. Dissecting

734 aggresome-targeting and aggregation signals in synphilin 1. *Journal of Biological Chemistry* **283**: 27575-27584.
735 https://doi.org/10.1074/jbc.M802216200

736 Zhao, L, Yang, Q, Zheng, J, Zhu, X, Hao, X, Song, J, Lebacq, T, Franssens, V, Winderickx, J, Nystrom, T, and
737 Liu, B. 2016. A genome-wide imaging-based screening to identify genes involved in synphilin-1 inclusion
738 formation in *Saccharomyces cerevisiae*. *Scientific Reports* **6**: 30134. https://doi.org/10.1038/srep30134

739

740 ## Figures and figure supplements

741 **Figure 1 SY1 aggregates mature into large IBs over time in normal cells, but this process is defective**
742 **in aged cells.**

743 **(A)** The maturation process of SY1 aggregates in yeast cells from scattered small aggregates to large single
744 IBs over time. DsRed-SY1 was expressed in yeast with the constitutive promoter TPI1, the phenotype of
745 SY1 aggregates was visualized at 4 h, 16 h and 48 h. Scale bar = 2 μm. **(B)** Cells with different phenotypes
746 of SY1 IBs are defined as three classes: Class 1 refers to only one IB in a cell, Class 2 refers to two IBs in a
747 cell, and Class 3 indicates three or more IBs in a cell. Scale bar = 2 μm. **(C)** Time-course study showing that
748 SY1 aggregates mature after 24 h of cultivation, when the cells have traversed the diauxic shift to enter the
749 respiratory and stationary growth phase. IBs were examined every 4 h from 4 to 48 h; green bars indicate
750 percentage of Class 3; white bars indicate percentage of Class 2; red bars indicate percentage of Class 1; the
751 purple curve indicates the optical density of the cell culture, indicated by the vertical axis on the right. **(D)**
752 Maturation of SY1 IBs was defective in old yeast cells. Scale bar = 5 μm. **(E)** The proportion of cells with
753 SY1 IBs was increased in old cells (61%) compared to young cells (27%). **(F)** The number of SY1 IBs in a
754 cell was increased in young cells (2.64±1.29) versus old cells (4.91±3.32).

755

756 **Figure 2 Genome-wide high-content imaging screen identifying the serine C-palmitoyltransferase**
757 **complex (SPT) as a modulator of SY1 inclusion maturation.**

758 **(A)** Schematic workflow for identifying mutants that regulate SY1 inclusion maturation. **(B)** The GO
759 enrichment analysis of genes whose mutants exhibited increased SY1 Class 3 aggregates (ClueGO, cut-off:
760 $P < 0.05$). **(C)** The network of the most enriched modules obtained above in 2B. **(D-E)** The increased SY1
761 Class 3 aggregates in the SPT mutant (*lcb1-4, lcb2-1, tsc3-2*) were rescued by backer-introducing the
762 corresponding wild-type gene (a MoBY plasmid carries a WT gene, and p5472 is the empty vector control).
763 Representative images from three independent experiments are shown in D, and quantifications were shown

764 in E. Scale bar = 2 μm.

765

766 **Figure 3 Sphingolipids regulate SY1 IB maturation and cytotoxicity in yeast cells.**

767 **(A)** A schematic diagram of the sphingolipid pathway in yeast cells. Myriocin blocks sphingolipid synthesis
768 via inhibition of the serine C-palmitoyltransferase (SPT) complex. **(B-C)** Dihydrosphingosine (DHS)
769 supplementation rescued the deficiency of SY1 IBs maturation in SPT mutants (*lcb1-4, lcb2-1, tsc3-2*).
770 Representative images from three independent experiments are shown in B, and quantifications are shown
771 in C. Scale bar = 2 μm. **(D-E)** Blocking intracellular sphingolipid synthesis with myriocin resulted in
772 defective maturation of SY1 IBs, and exogenous addition of DHS could reverse the effect of myriocin.
773 Representative images from three independent experiments are shown in D, and quantifications are shown
774 in E. Scale bar = 2 μm. **(F)** DHS ameliorated the cytotoxicity of SY1 in SPT mutants (*lcb1-4, lcb2-1, tsc3-*
775 *2*).

776

777 **Figure 4 SY1 IBs associate with mitochondria in yeast cells.**

778 **(A)** SY1 IBs had no obvious association with the plasma membrane (Pma1-GFP), vacuoles (Vph1-GFP), or
779 ER (Sec63-GFP), but were strongly associated with mitochondria (Tom70-GFP) (See also Figure 4-figure
780 supplement 1A). Scale bar = 2 μm. **(B)** MitoTracker probe confirmed that all the three classes of IBs were
781 closely associated with mitochondria (See also Figure 4-figure supplement 1B). Scale bar = 2 μm. **(C)** Super-
782 resolution microscopy and 3D-SIM construction demonstrated that the SY1 IBs are packed and surrounded
783 by mitochondria. Scale bar = 1 μm. **(D)** Co-immunoprecipitation assays showing that SY1 physically binds
784 to several mitochondrial membrane proteins, including Tom70, Tom37 and Tim44. The yeast mitochondrial
785 membrane proteins Tom70, Tom37, Sam35 and Tim44 were individually C-terminally tagged with GFP, and
786 the strains were then transformed with a control plasmid (Vector) or a SY1-overproducing plasmid (SY1),
787 respectively. Cells were grown for 24 h and harvested for subsequent IP experiments. **(E-F)** The association
788 of SY1 IBs with mitochondria decreases when the physical interaction between SY1 and mitochondrial
789 membrane proteins is disrupted (*tom70Δ*, *tom37Δ*, *tim44*). Representative images from three independent
790 experiments are shown in E and quantifications are shown in F. Scale bar = 2 μm.

791 **Figure 4-figure supplement 1. Statistics of SY1 IBs surrounded by cellular organelles.**

792 **(A)** Statistics of the proportion of SY1 IBs surrounded by different organelles, corresponding to Fig 4A. **(B)**
793 Statistics of the proportion of three different classes of SY1 IBs surrounded by mitochondria, corresponding
794 to Fig 4B. n.s., not statistically significant.

795 **Figure 4-figure supplement 2. IBs of TDP43, FUS1 and Htt103Qp interact with mitochondria.**
796 Shown are the IBs formed by TDP43, FUS1 and Htt103Qp when fused to GFP and their co-localization with
797 Tom70, which was genomically tagged with RFP. Scale = 2 μm.

798

799 **Figure 5 Sphingolipids regulate SY1-induced mitochondrial toxicity in yeast cells.**

800 **(A)** Overexpression of SY1 decreased mitochondrial membrane potential (indicated by Rho 123 fluor
801 intensity), increased cellular ROS levels (indicated by DCF mean intensity) and reduced cell viability
802 (indicated by ATP level) in yeast cells. (**B)** Effects of myriocin treatment on SY1 cytotoxicity in yeast cells
803 as judged by mitochondrial membrane potential / ROS levels / cell viability). **(C)** Effects of exogenous
804 addition of DHS on SY1 cytotoxicity in yeast cells based on mitochondrial membrane potential / ROS levels
805 / cell viability.

806 **Figure 5-figure supplement 1. The effect of myriocin (A) and DHS (B) treatment on SY1 protein**
807 **expression in yeast cells.**
808 SY1 expression was examined by Western blot analysis in samples prepared from cells used in the
809 experiments corresponding to Fig. 5B and Fig. 5C respectively. n.s., not statistically significant.

810

811 **Figure 6 SPTLC2 knockout alters the morphology of SY1 IBs and increases the cytotoxicity in**
812 **mammalian cells.**

813 **(A)** The 3D reconstruction showed that SY1 IBs were associated with mitochondria in mammalian HEK293t
814 cells. GFP-SY1 was expressed in HEK293t cells and mitochondria were probed with MitoTracker. The 3D
815 structure was constructed using Imaris software. Scale bar = 10 μm. **(B)** SY1 expression decreased
816 mitochondrial function in HEK293t cells. Mitochondrial membrane potential was monitored by JC-1
817 staining, ROS levels were determined by DCF mean intensity values, mitochondrial superoxide was
818 analyzed by MitoSOX mean intensity values. **(C)** The 3D structures of spherical and irregular SY1 IBs, as
819 well as their interaction with mitochondria was visualized using Imaris software (See also Figure 6-figure

820 supplement 2). **(D)** SPTLC2 knockout HEK293t cells had impaired management of SY1 IBs, with increased
821 dispersed irregular IB structures. Scale bar = 20 μm. **(E)** SPTLC2 knockout increased SY1 cytotoxicity. Cell
822 viability (indicated by luminescence) / ROS (indicated by DCF mean intensity) / mitochondrial membrane
823 potential (indicated by JC-1 staining) assays were analyzed.

824 **Figure 6-figure supplement 1. SPTLC2-Knockout by CRISPR/Cas9 genome editing.**

825 **(A)** The experimental flow chart for SPTLC2 knockout in HEK293t cells using CRISPR/Cas9. **(B)** The
826 sequencing results of the corresponding deletion sites of two obtained knockout cell lines.

827 **Figure 6-figure supplement 2. Statistics of SY1 IB formation.**

828 Statistics of SY1 IB formation in wild type HEK293t and SPTLC2 knockout cells.

829 **Figure 6-figure supplement 3. The expression of SY1 protein.**

830 The expression of SY1 protein in HEK293t SPTLC2 knockout cells. n.s., not statistically significant.

831

832 **Figure 7 Sphingolipids regulate SY1-induced cytotoxicity and SY1 IB morphology in mammalian cells.**

833 **(A)** Inhibition of the intracellular sphingolipid synthesis pathway by myriocin enhanced SY1 cytotoxicity
834 based on ATP content, intracellular ROS levels and mitochondrial membrane potential assays. **(B)** Addition
835 of exogenous DHS rescued the cytotoxicity caused by SY1 expression. **(C)** Exogenous addition of DHS to
836 SPTLC2 knockout cells restored the typical spherical SY1 IBs in HEK293t. Statistics of the ratio of cells
837 with dispersed irregular IBs after exogenous addition of DMSO and DHS to HEK293t SPTLC2 knockout
838 cells (See also Figure 7-figure supplement 2). Scale bar = 20 μm. **(D)** DHS ameliorated SY1 cytotoxicity by
839 normalizing cell viability, intracellular ROS levels, and mitochondrial membrane potential.

840 **Figure 7-figure supplement 1. The expression of SY1 protein in HEK293t and SPTLC2 knockout**
841 **cells**

842 **(A-B)** The effect of myriocin (A) and DHS (B) treatment on SY1 expression in HEK293t cells. **(C)** The
843 effect of DHS treatment on SY1 expression in SPTLC2 knockout cells. n.s., not statistically significant.

844 **Figure 7-figure supplement 2. Statistics of SY1 IB formation.**

845 Statistics of the effect on SY1 IB formation in SPTLC2 knockout cells after exogenous addition of either
846 DMSO or DHS.

847

Figure 1

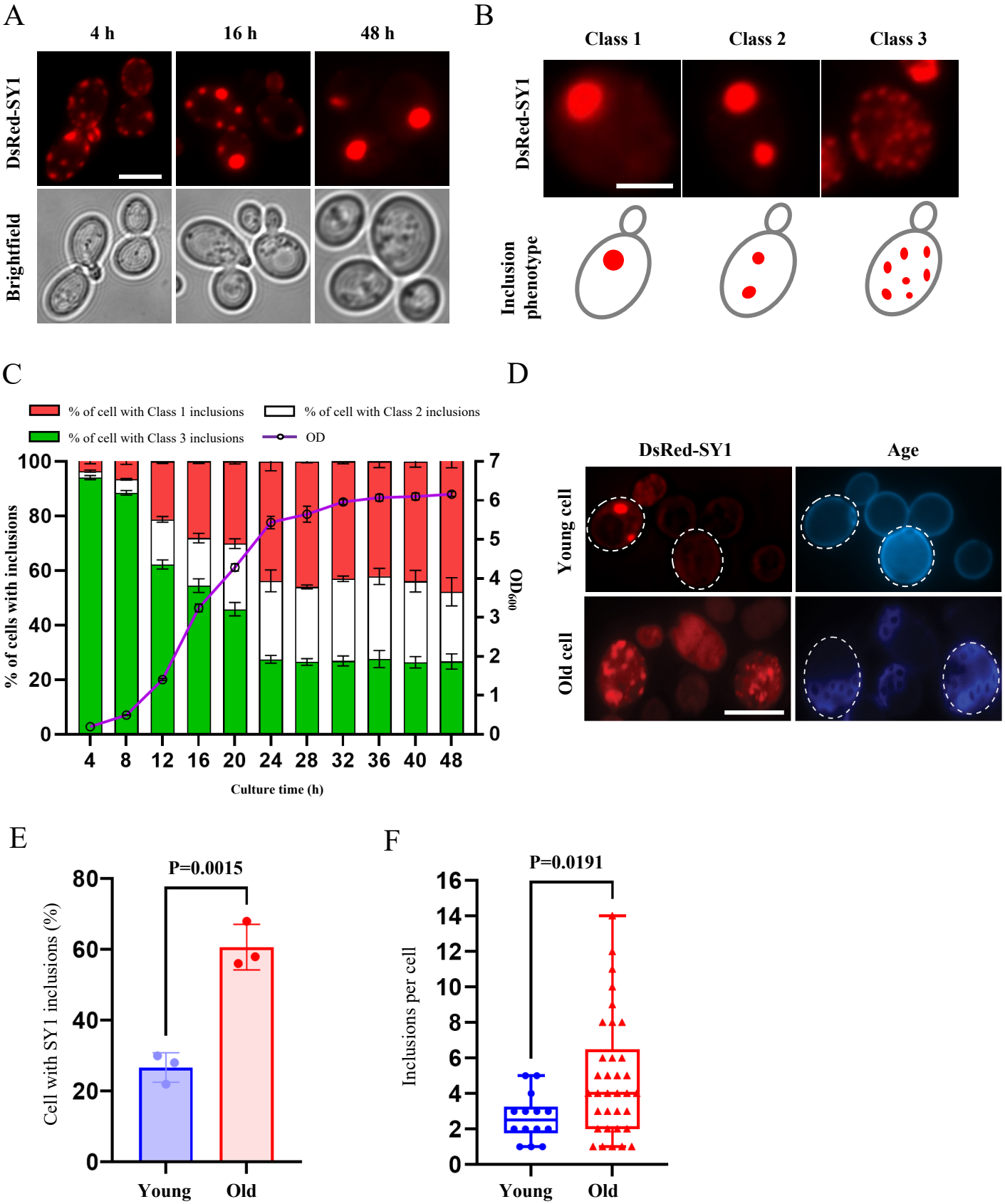
A
4 h
16 h
48 h
DsRed-SY1
Brightfield
B
Class 1
Class 2
Class 3
DsRed-SY1
Inclusion phenotype
C
% of cell with Class 1 inclusions
% of cell with Class 2 inclusions
% of cell with Class 3 inclusions
OD
% of cells with inclusions
OD600
Culture time (h)
D
DsRed-SY1
Age
Young cell
Old cell
E
P=0.0015
Cell with SY1 inclusions (%)
Young
Old
F
P=0.0191
Inclusions per cell
Young
Old

Figure 2

A

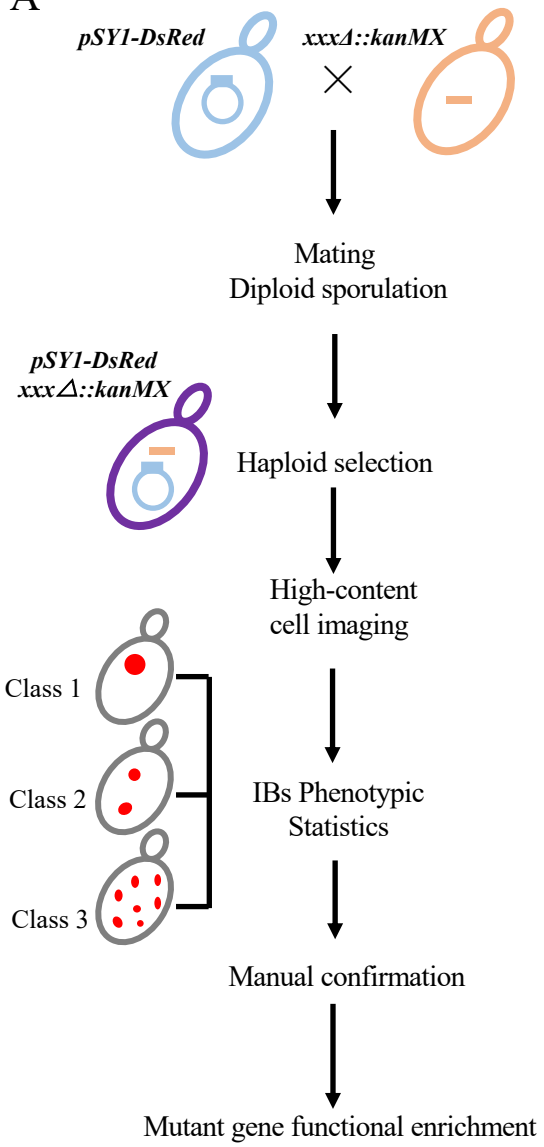

B

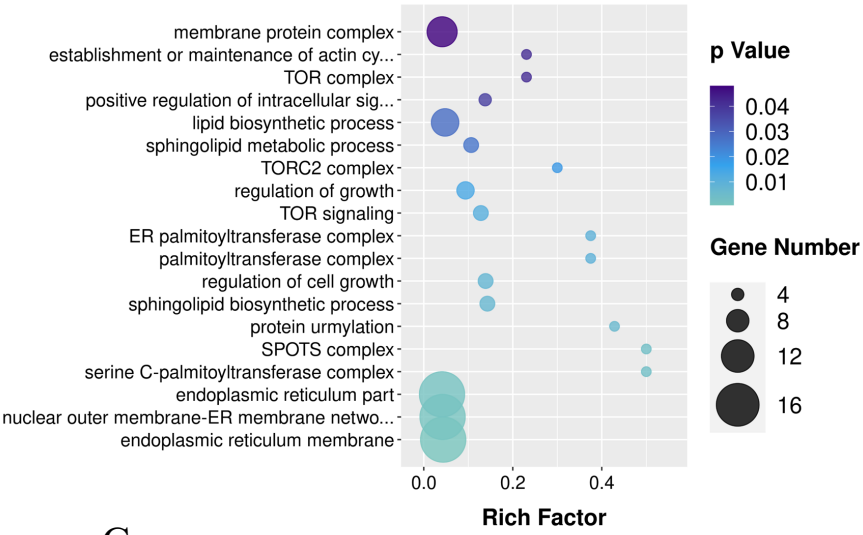

C

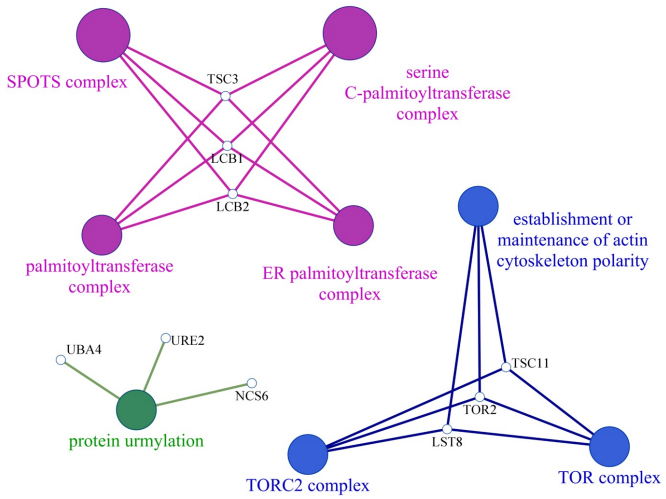

D

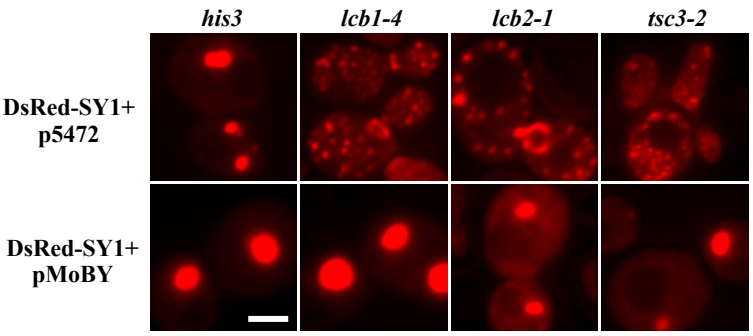

E

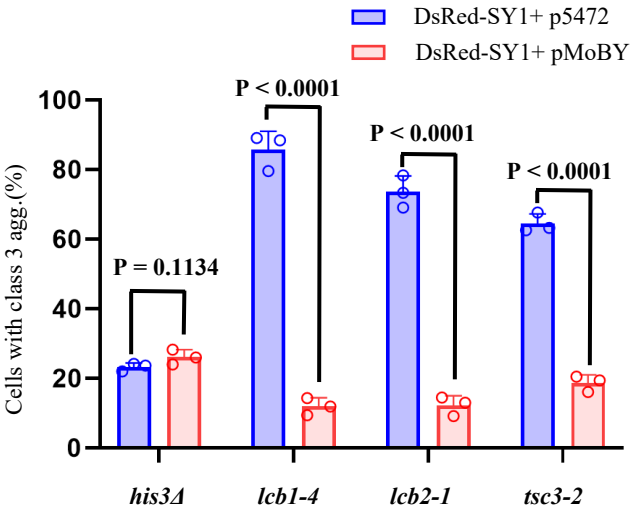

Figure 3

A

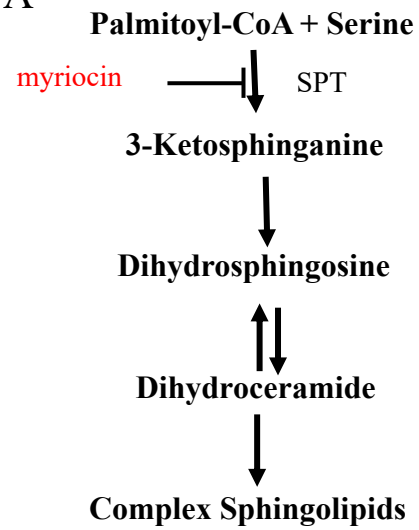

B

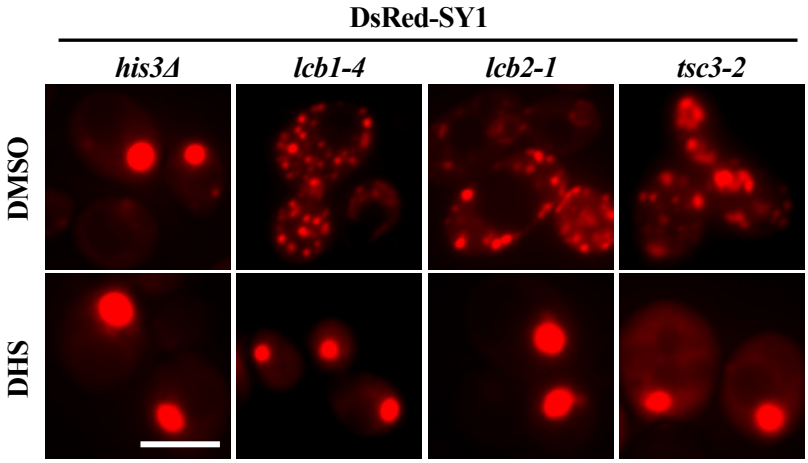

C

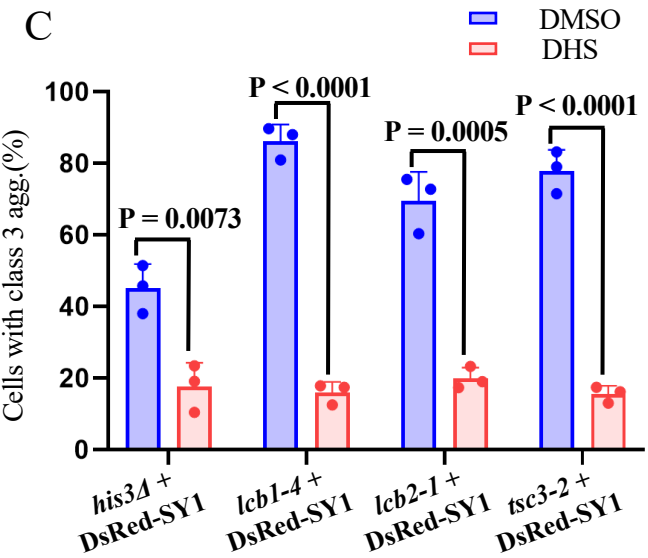

D

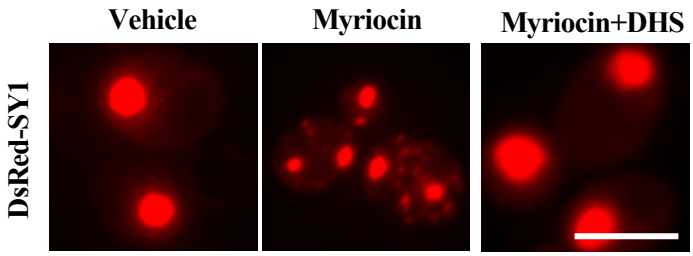

E

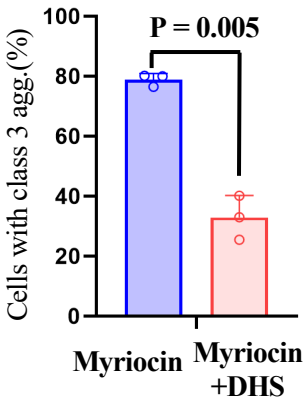

F

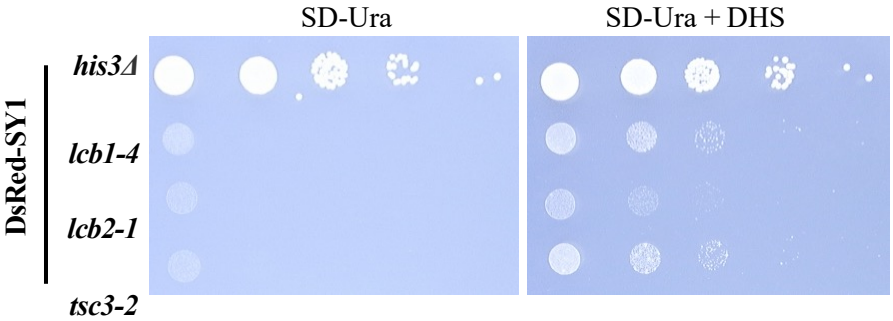

Figure 4

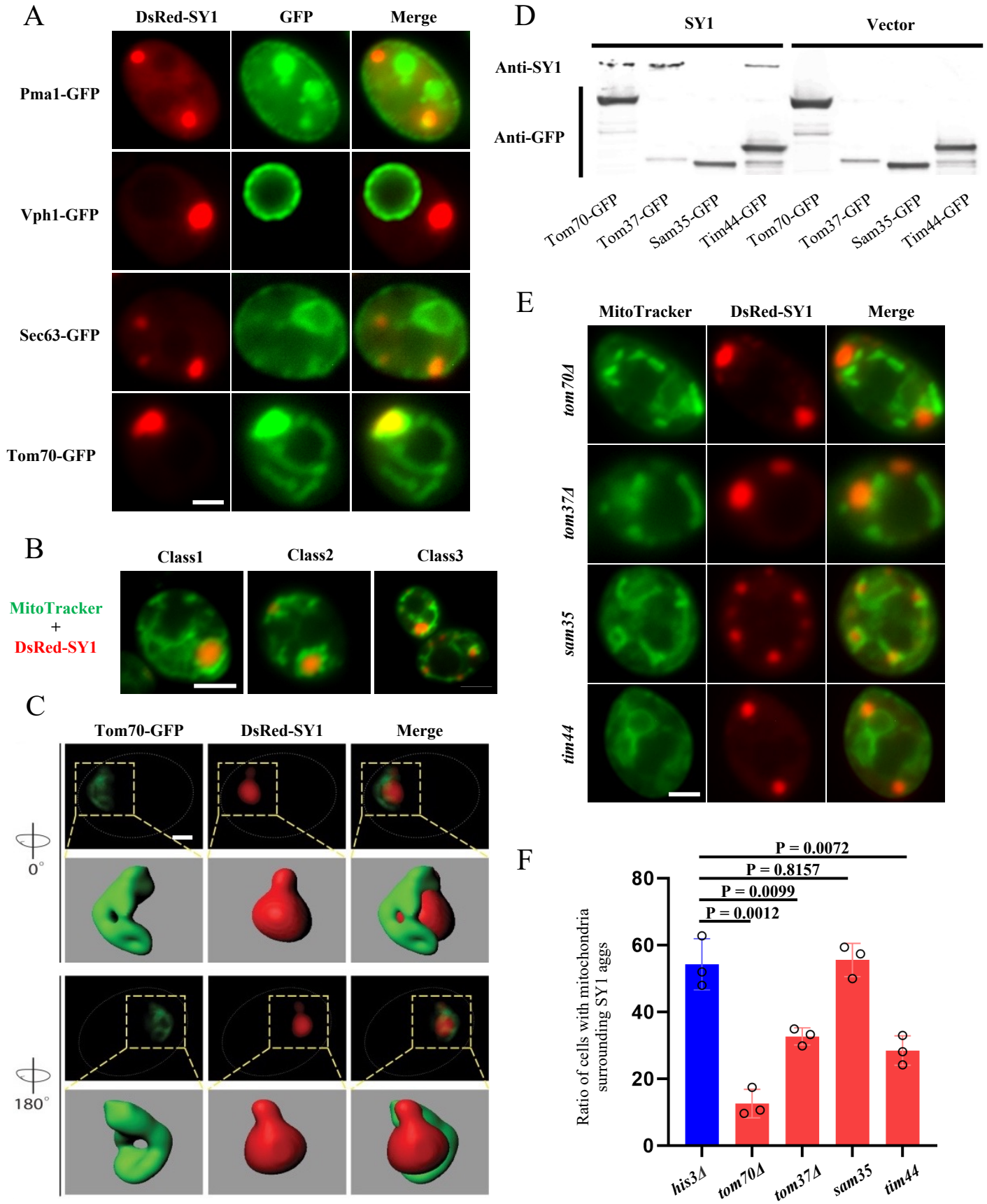
A
DsRed-SY1
GFP
Merge
Pma1-GFP
Vph1-GFP
Sec63-GFP
Tom70-GFP
B
Class1
Class2
Class3
MitoTracker
+
DsRed-SY1
C
Tom70-GFP
DsRed-SY1
Merge
0°
180°
D
SY1
Vector
Anti-SY1
Anti-GFP
Tom70-GFP
Tom37-GFP
Sam35-GFP
Tim44-GFP
Tom70-GFP
Tom37-GFP
Sam35-GFP
Tim44-GFP
E
MitoTracker
DsRed-SY1
Merge
tom70Δ
tom37Δ
sam35
tim44
F
P = 0.0072
P = 0.8157
P = 0.0099
P = 0.0012
Ratio of cells with mitochondria surrounding SY1 aggs
80
60
40
20
0
his3Δ
tom70Δ
tom37Δ
sam35
tim44

Figure 5

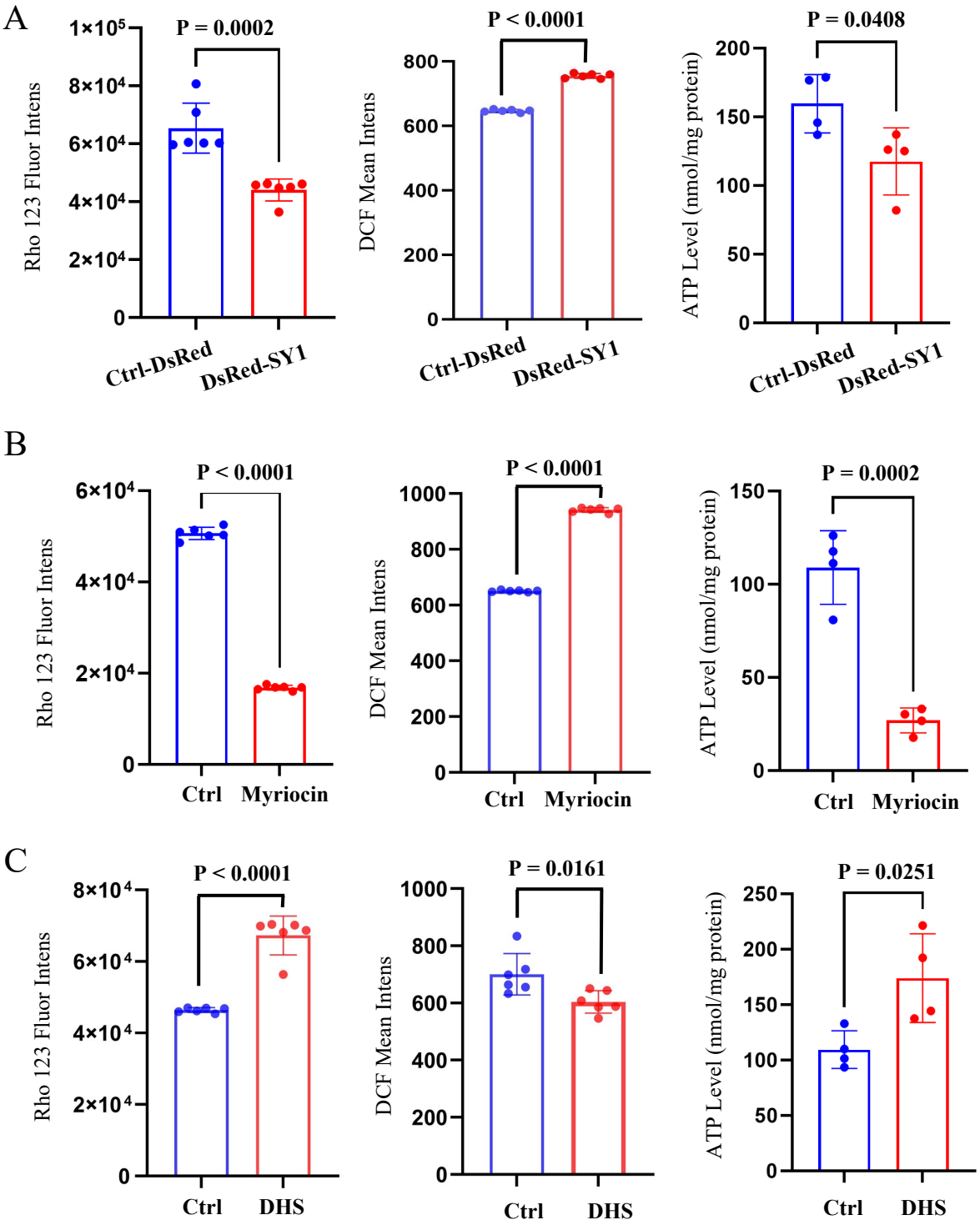
A
P = 0.0002
Rho 123 Fluor Intens
1×10⁵
8×10⁴
6×10⁴
4×10⁴
2×10⁴
0
Ctrl-DsRed
DsRed-SY1
P < 0.0001
DCF Mean Intens
800
600
400
200
0
Ctrl-DsRed
DsRed-SY1
P = 0.0408
ATP Level (nmol/mg protein)
200
150
100
50
0
Ctrl-DsRed
DsRed-SY1
B
P < 0.0001
Rho 123 Fluor Intens
6×10⁴
4×10⁴
2×10⁴
0
Ctrl
Myriocin
P < 0.0001
DCF Mean Intens
1000
800
600
400
200
0
Ctrl
Myriocin
P = 0.0002
ATP Level (nmol/mg protein)
150
100
50
0
Ctrl
Myriocin
C
P < 0.0001
Rho 123 Fluor Intens
8×10⁴
6×10⁴
4×10⁴
2×10⁴
0
Ctrl
DHS
P = 0.0161
DCF Mean Intens
1000
800
600
400
200
0
Ctrl
DHS
P = 0.0251
ATP Level (nmol/mg protein)
250
200
150
100
50
0
Ctrl
DHS

Figure 6

A

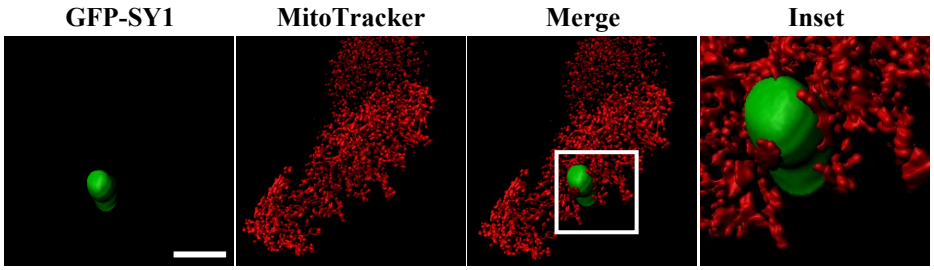

C

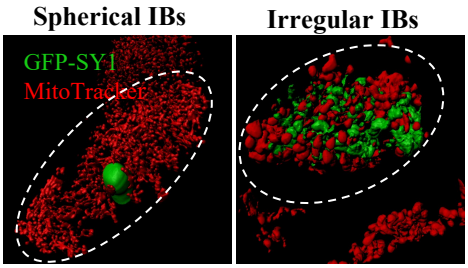

B

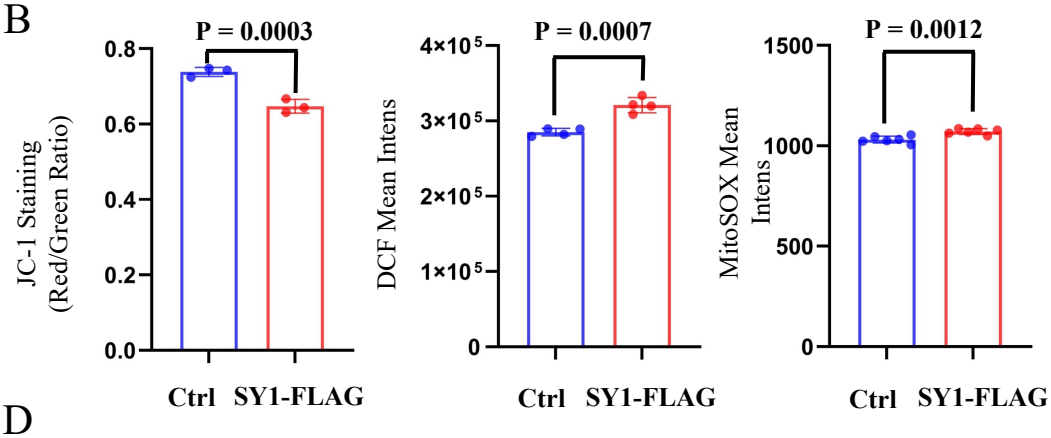

D

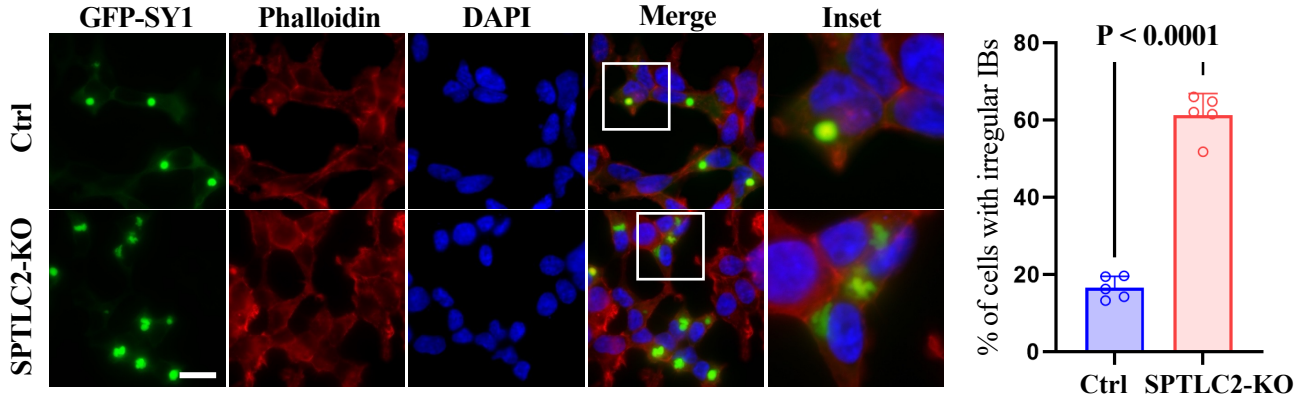

E

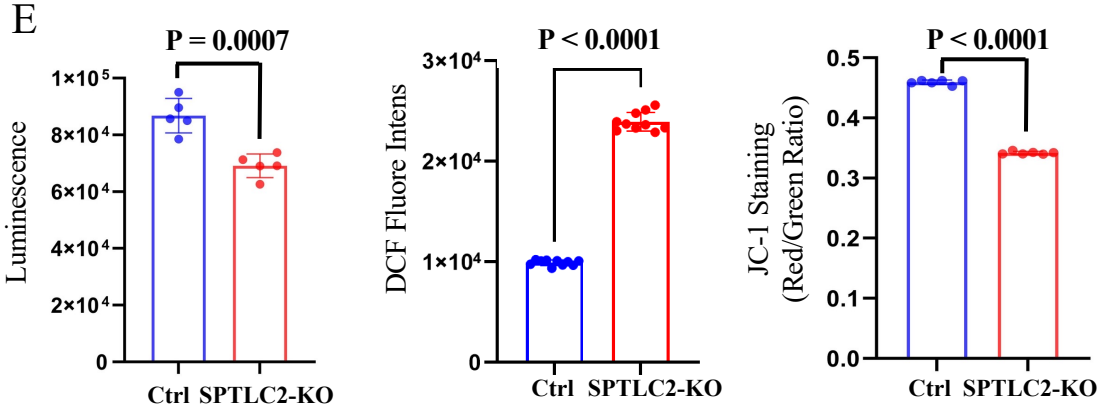

Figure 7

A

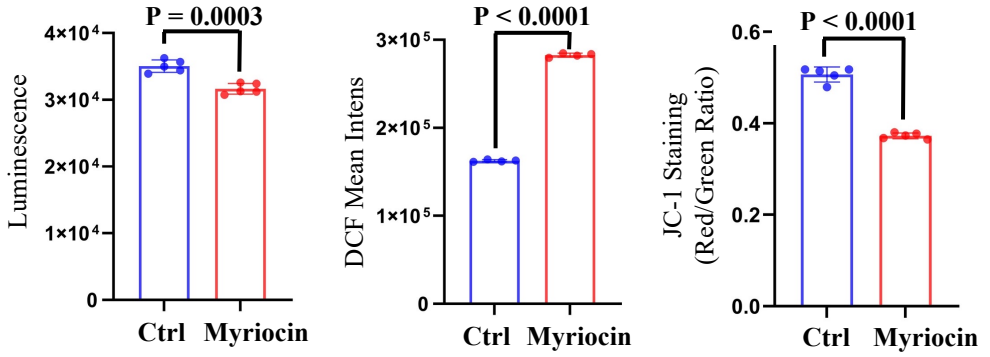

B

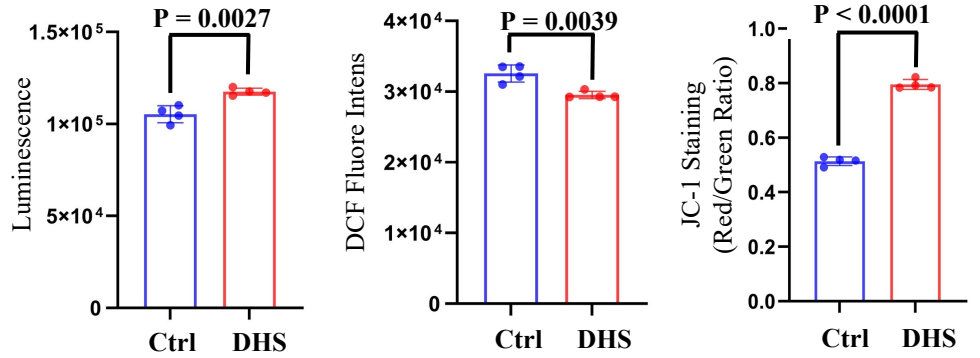

C

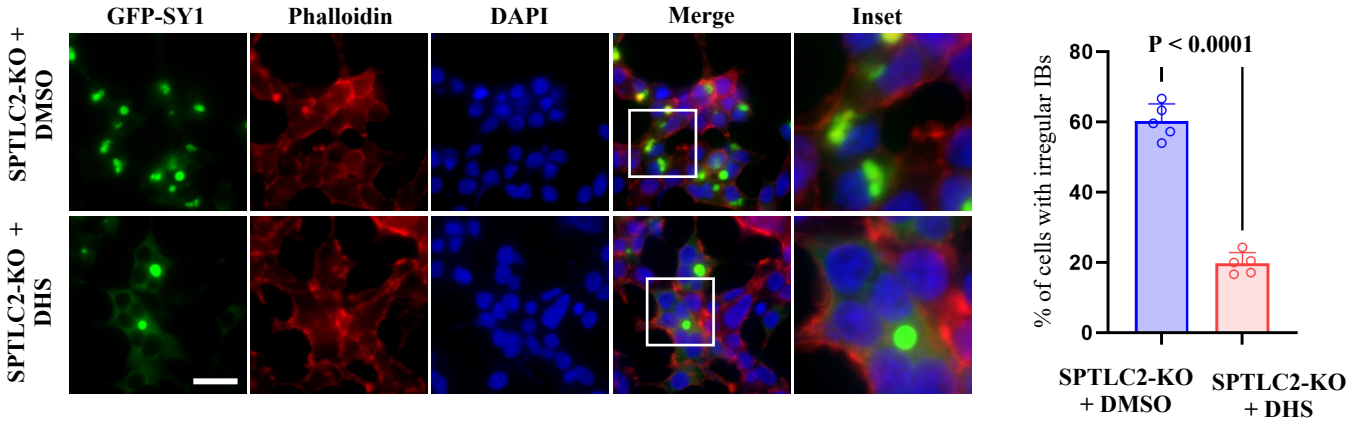
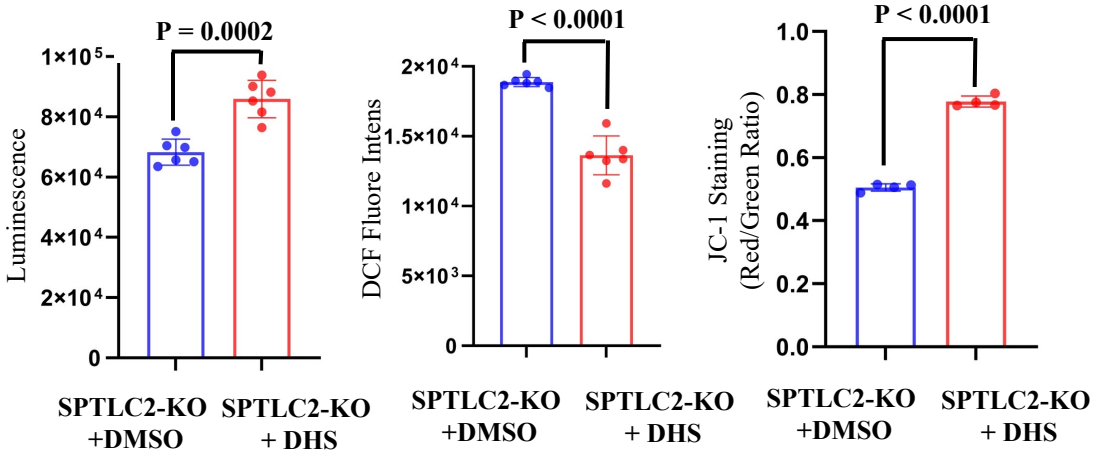
D